JGR Space Physics

RESEARCH ARTICLE
10.1029/2020JA029095

Special Section:
Geospace multi-point observations in Van Allen Probes and Arase era

Magnetic Field and Energetic Particle Flux Oscillations and High-Frequency Waves Deep in the Inner Magnetosphere During Substorm Dipolarization: ERG Observations

Yukinaga Miyashita[1,2], Tzu-Fang Chang[3], Yoshizumi Miyoshi[4], Tomoaki Hori[4], Akira Kadokura[5], Satoshi Kasahara[6], Shiang-Yu Wang[7], Kunihiro Keika[6], Ayako Matsuoka[8], Yoshimasa Tanaka[5], Yoshiya Kasahara[9], Mariko Teramoto[10], Chae-Woo Jun[4], Kazushi Asamura[11], Yoichi Kazama[7], Sunny W. Y. Tam[3], Bo-Jhou Wang[7], Shoichiro Yokota[12], Atsushi Kumamoto[13], Fuminori Tsuchiya[14], Masafumi Shoji[4], Satoshi Kurita[15], Shun Imajo[8], and Iku Shinohara[11]

[1]Space Science Division, Korea Astronomy and Space Science Institute, Daejeon, South Korea, [2]Department of Astronomy and Space Science, Korea University of Science and Technology, Daejeon, South Korea, [3]Institute of Space and Plasma Sciences, National Cheng Kung University, Tainan, Taiwan, [4]Institute for Space-Earth Environmental Research, Nagoya University, Nagoya, Japan, [5]National Institute of Polar Research, Tachikawa, Japan, [6]Department of Earth and Planetary Science, Graduate School of Science, The University of Tokyo, Bunkyo, Japan, [7]Academia Sinica Institute of Astronomy and Astrophysics, Taipei, Taiwan, [8]Data Analysis Center for Geomagnetism and Space Magnetism, Graduate School of Science, Kyoto University, Kyoto, Japan, [9]Graduate School of Natural Science and Technology, Kanazawa University, Kanazawa, Japan, [10]Faculty of Engineering, Kyushu Institute of Technology, Kitakyusyu, Japan, [11]Institute of Space and Astronautical Science, Japan Aerospace Exploration Agency, Sagamihara, Japan, [12]Department of Earth and Space Science, Graduate School of Science, Osaka University, Toyonaka, Japan, [13]Department of Geophysics, Graduate School of Science, Tohoku University, Sendai, Japan, [14]Planetary Plasma and Atmospheric Research Center, Graduate School of Science, Tohoku University, Sendai, Japan, [15]Research Institute for Sustainable Humanosphere, Kyoto University, Uji, Japan

Abstract Using Exploration of energization and Radiation in Geospace (ERG or Arase) spacecraft data, we studied low-frequency magnetic field and energetic particle flux oscillations and high-frequency waves deep in the inner magnetosphere at a radial distance of ~4–5 R_E during substorm dipolarization. The magnetic field oscillated alternately between dipole-like and taillike configuration at a period of ~1 min during dipolarization. When the magnetic field was dipole-like, the parallel magnetic component of the Pi2 waves was at trough. Both energetic ion and electron fluxes with a few to tens of kiloelectronvolts enhanced out of phase, indicating that magnetosonic waves were in slow mode. Field-aligned currents also oscillated. These observations are consistent with signatures of ballooning instability. In addition, we found that broadband waves from the Pi1 range to above the electron cyclotron frequency tended to appear intermittently in the central plasma sheet near dipole-like configuration.

Plain Language Summary Dipolarization is an important magnetospheric process for substorm onset and development, but its mechanism has not been well understood yet. Using spacecraft data, we studied low-frequency magnetic field and energetic particle flux oscillations and high-frequency waves deep in the inner magnetosphere during substorm dipolarization. The present results will shed light on instabilities causing substorm dipolarization.

Key Points:
- The magnetic field and particle fluxes oscillated deep in the inner magnetosphere during substorm dipolarization
- These signatures are consistent with those of ballooning instability
- Simultaneously high-frequency waves appeared intermittently near dipole-like configuration

Supporting Information:
Supporting Information may be found in the online version of this article.

Correspondence to:
Y. Miyashita,
miyasita@kasi.re.kr

Citation:
Miyashita, Y., Chang, T.-F., Miyoshi, Y., Hori, T., Kadokura, A., Kasahara, S., et al. (2021). Magnetic field and energetic particle flux oscillations and high-frequency waves deep in the inner magnetosphere during substorm dipolarization: ERG observations. *Journal of Geophysical Research: Space Physics*, *126*, e2020JA029095. https://doi.org/10.1029/2020JA029095

Received 30 DEC 2020
Accepted 12 AUG 2021

1. Introduction

The substorm-triggering mechanism is a major issue in magnetospheric research. During substorms various phenomena occur in the magnetosphere, in the ionosphere, and on the ground. Among them, magnetic reconnection and current disruption/dipolarization in the near-Earth magnetotail are important for substorm triggering (e.g., Baker et al., 1996; Lui, 1996), but their mechanisms, as well as their causal relationship, are not fully understood yet.

A main candidate for causing current disruption/dipolarization is ballooning instability (e.g., Bhattacharjee et al., 1998; Chang & Cheng, 2015; Chen et al., 2003; Cheng & Lui, 1998; Erickson et al., 2000; Kalmoni et al., 2015; Nishimura et al., 2016; Park et al., 2010; Pu et al., 1997, 1999; Roux et al., 1991; Saito et al., 2008; Samson et al., 1996; Voronkov et al., 1997; Xing et al., 2013). It is related to low-frequency waves at 1–2 min or Pi2 period range. Previous studies showed that the magnetic field and particle fluxes oscillated at ~1–2 min period at geosynchronous orbit (Holter et al., 1995; Roux et al., 1991; Saka et al., 1999) and at larger distances of $R \sim 8$ and 11 R_E (Keiling et al., 2008a, 2008b) at and during dipolarization. These oscillations are correlated with ground Pi2 pulsations at high and low latitudes, modulation of auroral brightening, and wave-like (bead-like) structure of the auroral onset arc (e.g., Keiling et al., 2008a, 2008b; Saka et al., 1999). Roux et al. (1991) and Keiling et al. (2008b) proposed that the oscillations are related to ballooning instability.

In the present study, we studied three dipolarization events that were observed by the Exploration of energization and Radiation in Geospace (ERG or Arase) spacecraft (Miyoshi et al., 2018c) deep in the inner magnetosphere at radial distances of $R \sim 4$–5 R_E. Here we analyzed not only magnetic field and particle oscillations at the Pi2 frequency range but also higher-frequency waves from the Pi1 range to above the electron cyclotron frequency. We found that signatures of ballooning instability were observed deep in the inner magnetosphere, accompanied by intermittent high-frequency waves.

2. Observations

We selected three dipolarization events, where the ERG footprint was in the field of view of an all-sky camera at Syowa (SYO) station in Antarctica (−66.60° geomagnetic latitude and 72.24° geomagnetic longitude). Of the selected events, we show the June 30, 2017 event in detail, while we show the June 17 and September 2, 2017 events briefly.

2.1. The June 30, 2017 Event

Figure 1 shows selected auroral images obtained by a white-light all-sky imager at Syowa for the June 30, 2017 event (see also Movie S1 for the full sequence). The auroral onset arc associated with the substorm, seen in the poleward part of the field of view, developed in four steps (cf. Mende et al., 2009; Miyashita & Ieda, 2018). Preonset auroral fading began in the eastern part of the auroral arc at 21:42:47 UT. At 21:44:04 UT initial brightening began at the same place as fading. The arc's wave-like structure grew gradually and then enhanced further in the middle of the arc at 21:59:21 UT. A few examples of bright spots constituting the wave-like structure are indicated by the small arrows in the 22:05:08 UT image. The luminosity oscillation at ~1–2 min period can also be seen in Figure S1. Finally, poleward expansion began in the middle of the arc at 22:10:31 UT. In this event, the aurora suddenly expanded equatorward from the poleward edge of the field of view at 22:16:43 UT, similarly to north-south aurora reported by Nakamura et al. (1993). This aurora spread extensively and reached ERG's footprint at 22:18:09 UT (see below for the timing). Here the times of initial brightening, enhancement of the wave-like structure, poleward expansion, and sudden equatorward expansion were determined by the method of Miyashita and Ieda (2018) that combines visual inspection of auroral images and a segmented (piecewise) linear fitting with one breakpoint for the count data (see Figure S1 for the fitting results). The interval of ~26 min from initial brightening to the beginning of poleward expansion for the present event was extremely longer than a typical interval of 30 s to 4 min (Lyons et al., 2002; Morioka et al., 2010). Since the luminosity of the onset arc tended to increase without suppression (see Figure S1), we conclude that the onset arc and its wave-like structure developed slowly for some reason.

We checked ground magnetic field data from Syowa (Yamamoto et al., 2008), as shown in Figure S2. The geomagnetic signatures of initial auroral brightening and enhancement of the wave-like structure were missed, probably because Syowa was located equatorward of the auroral onset arc. Small-amplitude Pi2 and Pi1 pulsations as well as the deflection of the D component due to field-aligned current began just after auroral poleward expansion. Just after auroral equatorward expansion, a large positive bay began, possibly due to enhanced field-aligned current, and Pi2 and Pi1 pulsations were amplified.

Figure 2 shows an overview of the June 30, 2017 dipolarization event observed by ERG deep in the inner magnetosphere at a radial distance of ~5.5 R_E (Miyoshi et al., 2018b). The top three panels show the

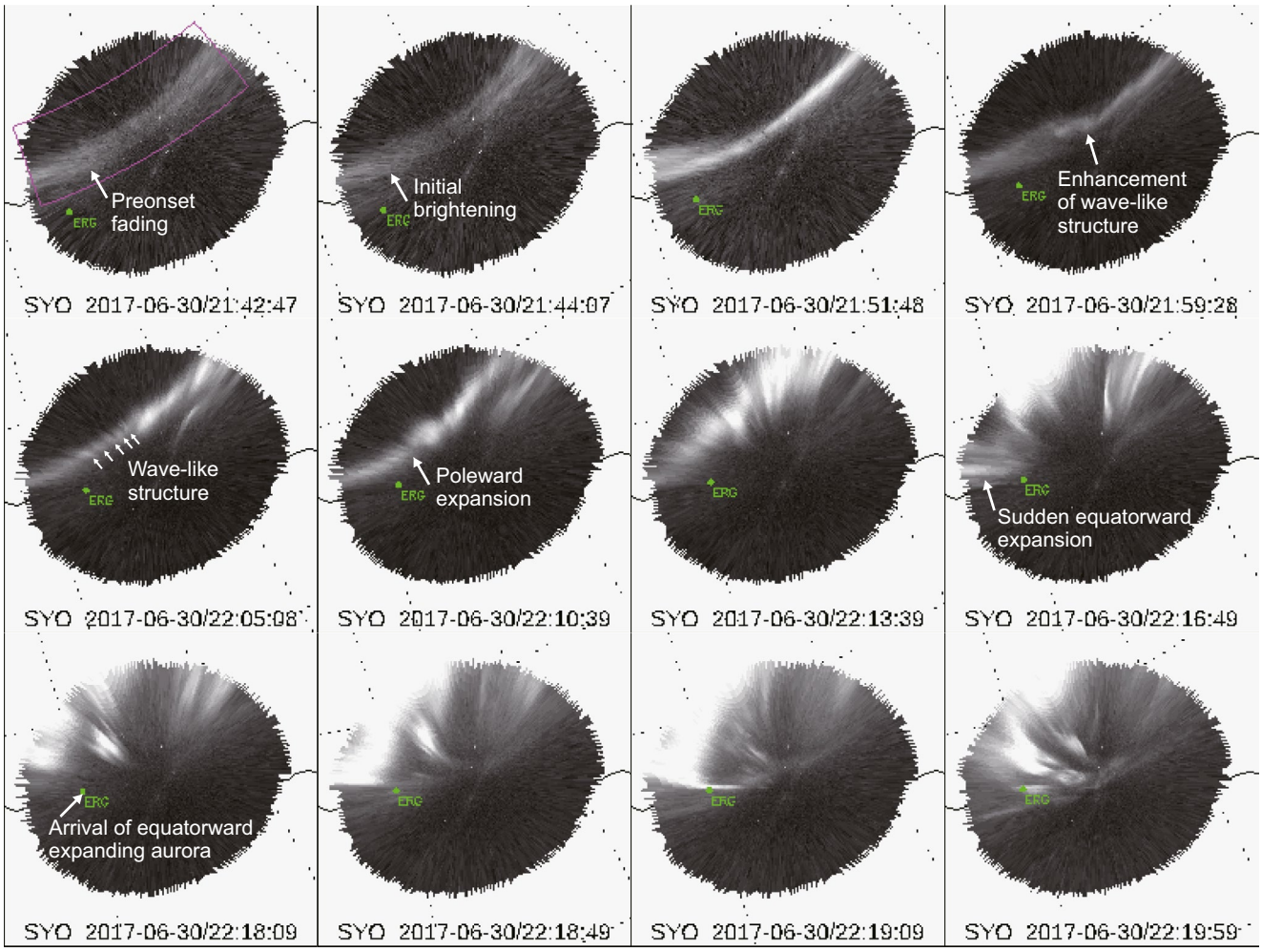

Figure 1. Auroral snapshots of the onset arc development for the June 30, 2017 event. The images were obtained by a white-light all-sky imager at Syowa. South (pole) is to the upper left, and west is to the upper right. The maximum count values of the black-white scale are set to 150 for the first three images and 255 for the later images. The green dot indicates Exploration of energization and Radiation in Geospace's (ERG) footprint calculated using the T96 magnetic field model (Tsyganenko, 1995). The large white arrows indicate approximate locations of the beginnings of the auroral steps. Average count variations for areas of 0.5° longitudinal width in the magenta box in the 21:42:47 UT image are shown in Figure S1. See Movie S1 for the full sequence.

magnetic field in *VDH* coordinates at 8 s resolution from the magnetic field experiment (MGF; Matsuoka et al., 2018b, 2018c), where the residuals after subtracting the thirteenth-generation International Geomagnetic Reference Field (IGRF; Alken et al., 2021) are shown. In the cylindrical *VDH* coordinate system, *H* is defined as being antiparallel to the dipole axis, *V* is radially outward and parallel to the magnetic equator, and *D* completes the right-hand orthogonal system (positive eastward). In this event, B_v was negative (earthward) throughout the interval. Dipolarization (persistent increase in the residual northward B_h and decrease in the residual radial $|B_v|$) began along with ~1 min period oscillations at ~22:18 UT, when the equatorward-expanding aurora reached ERG's footprint, consistent with Liou et al. (2002). Since ERG's footprint was located equatorward of the auroral onset arc (Figure 1), ERG observed inward expansion of the dipolarization region. Dipolarization ended at ~22:25 UT. ERG also observed oscillation of the residual B_d during dipolarization, probably due to field-aligned current oscillation.

The high-frequency electric field power spectrogram (Figure 2, the fourth panel) from the high-frequency analyzer (HFA; Kasahara et al., 2018e, 2021; Kumamoto et al., 2018) of the plasma wave experiment (PWE; Kasahara et al., 2018c) shows that until 21:47 UT the upper hybrid resonance frequency was ~60 kHz, which corresponds to the electron number density of ~40 cm^{-3}, and then the upper hybrid resonance frequency (the electron number density) decreased between 21:47 and 21:49 UT (see also Figure S3). This decrease

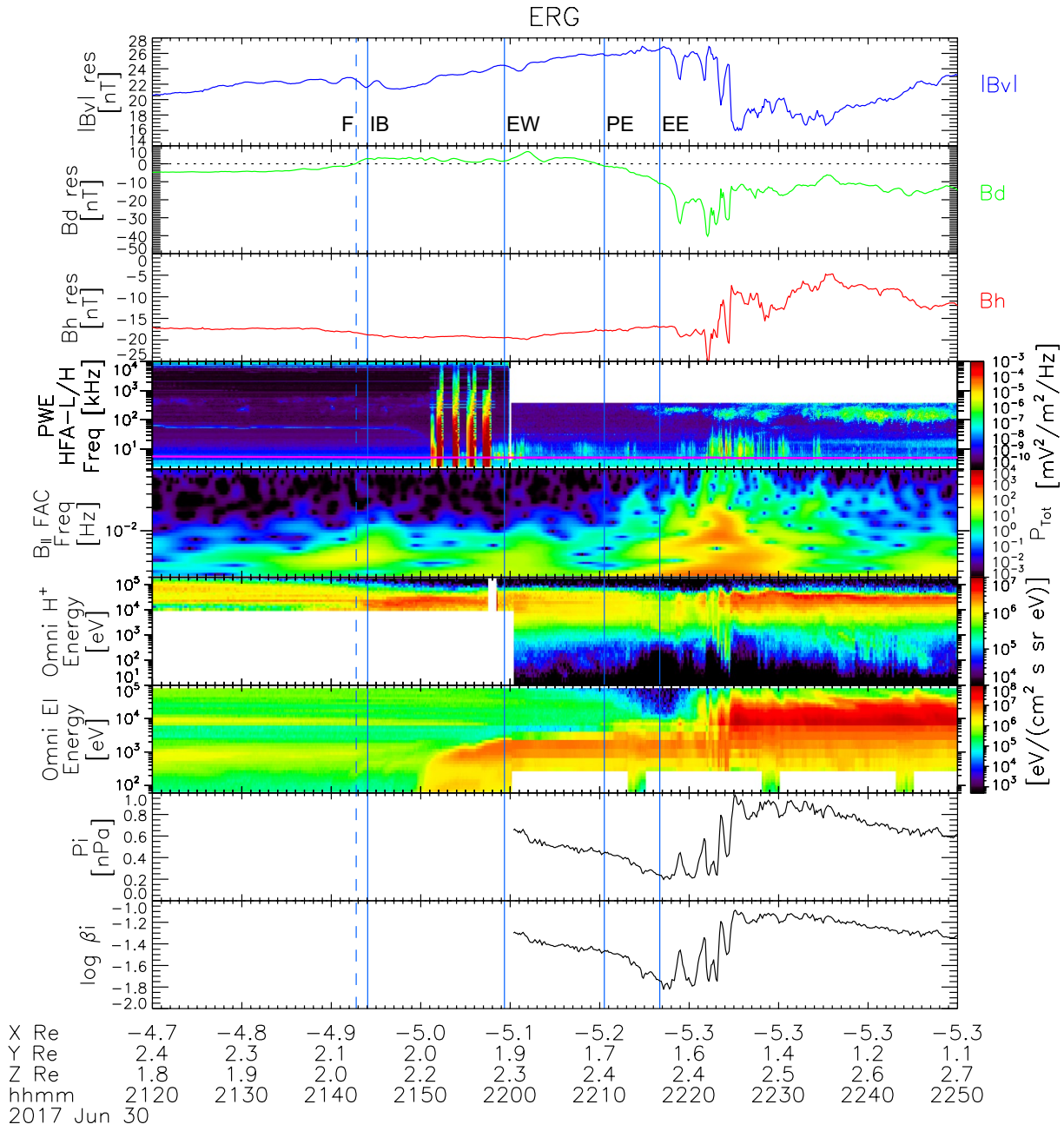

Figure 2. Exploration of energization and Radiation in Geospace (ERG) magnetic field, wave, and particle data from 21:20 to 22:50 UT on June 30, 2017. From top to bottom shown are the residual earthward ($|B_v|$), eastward (B_d), and northward (B_h) magnetic field after subtracting the International Geomagnetic Reference Field (IGRF), electric field power spectrogram at high frequencies with the electron cyclotron frequency shown by the magenta line, wavelet scalogram for the parallel component of the wave magnetic field at low frequencies, proton and electron omnidirectional spectrograms for medium and low energies, the ion (proton) pressure, and the ion β. The dashed vertical line indicates the beginning of preonset auroral fading (F). The solid vertical lines from the left indicate the beginnings of initial auroral brightening (IB), enhancement of the wave-like structure (EW), poleward expansion (PE), and sudden equatorward expansion (EE). The spacecraft position is shown at the bottom in solar magnetospheric (SM) coordinates.

indicates that ERG exited from the plasmasphere after initial brightening. Auroral kilometric radiation at ~100–200 kHz was seen after auroral poleward expansion. High-frequency waves at ~10 kHz around and above the electron cyclotron frequency (the magenta line) were also seen after ERG exited the plasmasphere, but they were more intense and broadband during dipolarization. Note that the intense broadband noises between 21:51 and 21:58 UT were artificial signals caused by PWE calibration. The wavelet scalogram for the wave magnetic field parallel to the ambient magnetic field (200 s running average) at low

frequencies from MGF (Figure 2, the fifth panel) shows that weak Pi2 pulsations in a lower frequency range of ~0.006–0.01 Hz appeared around initial auroral brightening and subsequent enhancement of wave-like auroral structure, and then intense Pi2 pulsations appeared after auroral poleward expansion. During dipolarization intense Pi2 pulsation in a high-frequency range of >~0.01 Hz and Pi1 (Pi1B) pulsations appeared.

Figure 2 (the sixth and seventh panels) shows proton and electron omnidirectional spectrograms for medium and low energies from the medium-energy particle experiments ion mass analyzer (MEP-i; Yokota et al., 2017, 2018), the low-energy particle experiments ion mass analyzer (LEP-i; Asamura, Kazama, et al., 2018; Asamura, Miyoshi, & Shinohara, 2018), the medium-energy particle experiments electron analyzer (MEP-e; Kasahara et al., 2018a, 2018b), and the low-energy particle experiments electron analyzer (LEP-e; Kazama et al., 2017; Wang et al., 2018). After plasmapause crossing at ~21:50 UT, ERG was in the plasma sheet. High-energy (>~10 keV) proton and electron fluxes decreased between ~22:10 UT and 22:19 UT, together with increase in the residual $|B_v|$, which was probably due to plasma sheet thinning. After a few transient high-energy proton and electron flux enhancements at ~22:19 to 22:24 UT, higher-energy proton and electron fluxes persistently enhanced. Accordingly, the ion (proton) pressure (the second panel from the bottom), derived by combining LEP-i and MEP-i data, also enhanced during dipolarization. These enhancements were probably caused by plasma sheet thickening and particle acceleration associated with dipolarization (Miyashita et al., 2010; Ohtani et al., 2002). The ion β (the bottom panel) was low, ~0.02–0.06, during this event.

Figure 3 shows the auroral count at ERG's footprint (±0.5° in magnetic latitude and ±2° in magnetic longitude) obtained from Syowa, the magnetic field, ion moments, and proton and electron spectrograms for medium and low energies at 0°, 90°, and 180° (±30°) pitch angles obtained by ERG during dipolarization. We can confirm that dipolarization and associated oscillation began at the same time as a large increase in the auroral count at ~22:18 UT due to the equatorward-expanding aurora. The magnetic field oscillated alternately between dipole-like and taillike configuration at ~1 min period during dipolarization. At most troughs of the parallel component of the wave magnetic field in the Pi2 frequency range (the sixth panel, the solid vertical lines), except for the first trough (the dashed vertical line), the residual northward B_h increased and the residual earthward $|B_v|$ decreased, that is, the magnetic field was dipole-like. On the other hand, at most peaks of the parallel component of the Pi2 wave, the magnetic field was taillike. Some peaks and troughs of B_h and $|B_v|$ did not necessarily occur exactly at the same time as those of the Pi2 waves, possibly because the observed waves were not necessarily purely in a single mode, due to mixture of some waves in another mode or fluctuations. At the first trough of the Pi2 wave, both northward and earthward components of the magnetic field decreased, possibly due to the explosive growth phase or rapid increase in the cross-tail current in the flux tube just outward of the ERG position (cf. Ohtani et al., 1992b).

The eastward magnetic field B_d (Figure 3, the fourth panel) oscillated during dipolarization. Comparing the Pi2 troughs and peaks, in most cases, B_d oscillations and Pi2 waves were in phase in the outer plasma sheet before ~22:20 UT, and after ERG entered the inner plasma sheet, they were out of phase. That is, in dipole-like configuration (the vertical lines), B_d deviated westward in the outer plasma sheet, while it deviated eastward in the inner plasma sheet. On the other hand, in taillike configuration (between the vertical lines), the deviations were in the opposite directions. As discussed later, these B_d oscillations were possibly generated by alternate changes of field-aligned currents. Meanwhile, we also checked the peaks and troughs of the B_d component, including those of rapid oscillation. In Figure S4, the solid magenta lines are drawn at the troughs in the outer plasma sheet and at the peaks in the inner plasma sheet, while the dashed magenta lines are drawn at the peaks in the outer plasma sheet and at the troughs in the inner plasma sheet. In addition to the above-mentioned tendency for the B_d peaks and troughs to be located near the Pi2 peaks and troughs, some B_d peaks and troughs can be seen between the Pi2 peak and trough.

The ion and electron spectrograms (Figure 3, the bottom six panels) show that at the troughs of the Pi2 wave, including the first trough, energetic ion and electron fluxes with a few to tens of kiloelectronvolts enhanced in parallel, antiparallel, and perpendicular directions, although this change does not seem clear for the second trough at ~22:20 UT. The ion and magnetic pressures in the Pi2 frequency range (the seventh panel) had nearly the same amplitudes and were out of phase during dipolarization. These out-of-phase oscillations indicate that the magnetosonic waves were in slow mode (cf. Holter et al., 1995; Southwood & Saunders, 1985). Furthermore, antiparallel (outward) low-energy proton fluxes, as well as parallel and

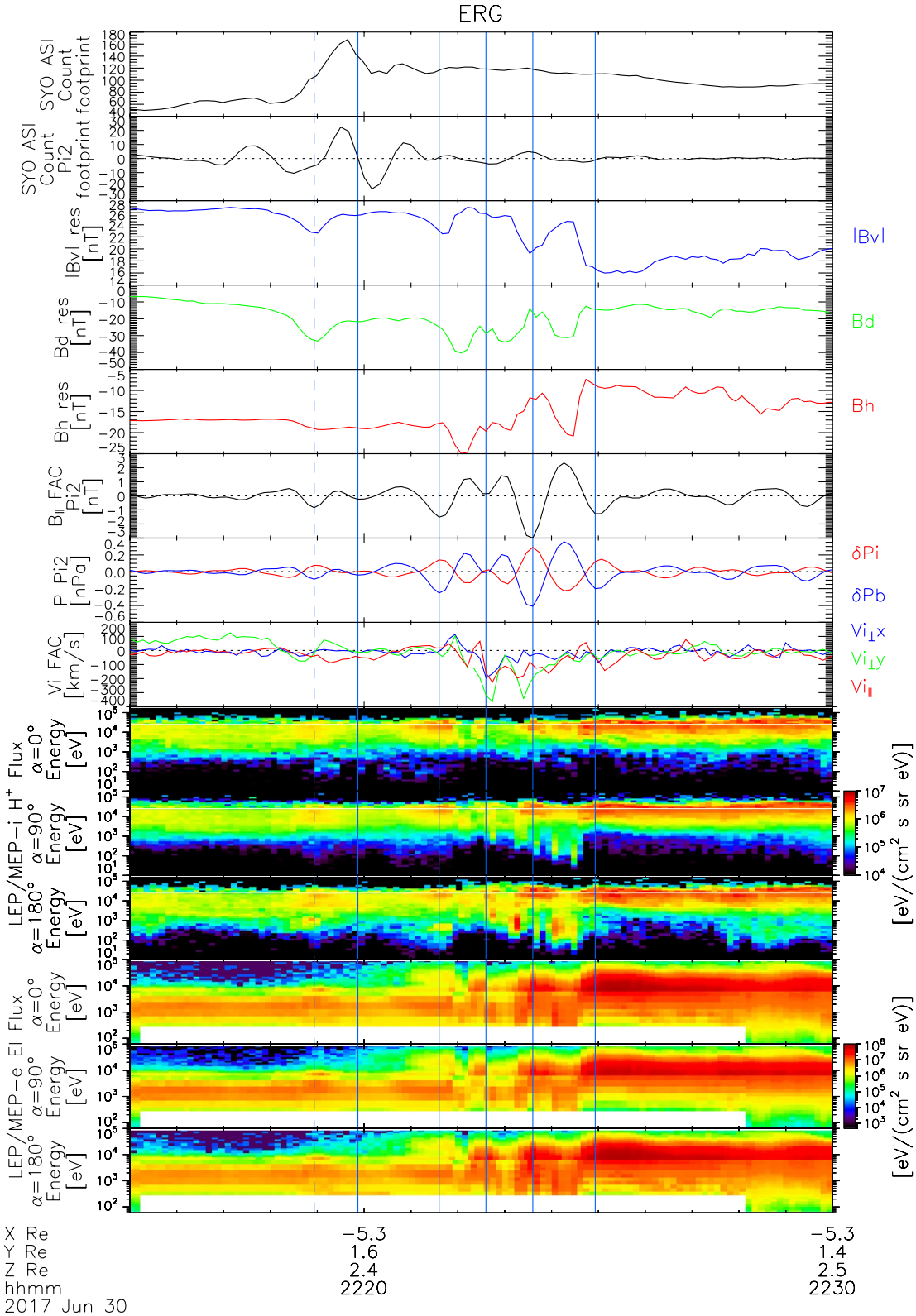

Figure 3.

antiparallel low-energy electron fluxes, enhanced periodically during dipolarization between 22:22 and 22:25 UT.

Figure 3 (the eighth panel) shows the ion (proton) velocities perpendicular and parallel to the magnetic field (in field-aligned coordinates, FAC) derived from LEP-i and MEP-i. Here the Z axis is in the ambient magnetic field direction (200 s running average), X is defined as the cross product of the negative azimuthal vector ($-\phi$, westward vector) of the spacecraft position in solar magnetospheric (SM) coordinates and Z (positive inward), and Y completes the orthogonal right-hand system and is on the plane defined by ϕ and Z (positive westward). Just after auroral poleward expansion, a westward flow at ~100 km/s persisted from ~22:12 to ~22:18 UT. At the beginning of dipolarization, the perpendicular ion flow was inward and westward, although it was not very fast. During dipolarization, the flow oscillated, and eastward flows reached –300 km/s. The behavior of these flows is similar to a flow pattern in a more outward region reported by Lee et al. (2012).

Figure 4 shows wave spectra in a frequency range of the Pi2 and Pi1 waves to megahertz. The magnetic and electric field spectra in the third and fourth panels, respectively, were taken from the onboard frequency analyzer of PWE (OFA-SPEC; Kasahara et al., 2018d; Matsuda et al., 2018), and the electric field spectra in the fifth panel were taken from the double probe of the electric field detector of PWE (EFD-DPB; Kasaba et al., 2017; Kasahara et al., 2019). The wavelet scalograms in the bottom three panels were obtained from the 64 Hz sampling magnetic field data from MGF (Matsuoka et al., 2018a) in field-aligned coordinates. During dipolarization, various kinds of wave appeared from low to high frequencies, such as Alfvén and magnetosonic Pi1 waves, electromagnetic waves below the electron cyclotron frequency, and electrostatic waves near and above the electron cyclotron frequency. The relatively intense Pi1 and higher-frequency waves tended to appear when the magnetic field was dipole-like (near the vertical lines), and they were more intense mainly in the central plasma sheet after ~22:22 UT. Note that all of these waves were not always observed at the same time. That is, all of these waves were observed in some times (the third and fourth solid lines), but only some of them were observed in the other times (the first, second, and last solid lines).

2.2. The September 2, 2017 Event

Although auroral data from Syowa for this event (Figures 5 and S5 and Movie S2) were contaminated by moonlight, auroral onset arc development was partially observed in the equatorward part of the field of view. Preonset fading possibly began in the eastern part of the arc at 22:15:49 UT. At 22:22:27 UT initial auroral brightening began at nearly the same place as fading. The arc's wave-like structure was not clearly seen, but the relatively bright spots indicated by the small black arrows in the 22:27:39 UT image possibly constituted wave-like structure. The luminosity oscillation at ~1–2 min period can be seen in Figure S5. Then poleward expansion began at 22:28:51 UT. The poleward-expanding aurora reached ERG's footprint in the western part of the field of view at 22:30:19 UT.

Ground magnetic field data from Syowa (Figure S6) show that a small negative excursion of the H component began just after initial auroral brightening, although Pi2 and Pi1 pulsations were not seen. About 2 min after auroral poleward expansion a large negative excursion began, reaching ~−300 nT and accompanied by Pi2 and Pi1 pulsations. The small and large negative excursions at initial brightening and poleward expansion, respectively, are consistent with the results of Morioka et al. (2010, 2014).

ERG was outside the plasmasphere (Figure S7) and in the outer plasma sheet or the plasma sheet boundary layer at $R \sim 4.2\ R_E$ until ~6 min after auroral poleward expansion (Figure 6, the sixth and seventh panels). The residual northward B_h (the third panel) as well as the proton and electron fluxes decreased due to

Figure 3. Auroral count at Exploration of energization and Radiation in Geospace's (ERG) footprint, and ERG magnetic field, wave, and particle data from 22:15 to 22:30 UT on June 30, 2017. Shown are (top and second panels) the auroral count and the component in the Pi2 frequency range at ERG's footprint (±0.5° in magnetic latitude and ±2° in magnetic longitude) obtained from Syowa, (third to fifth panels) the three components of the residual magnetic field, (sixth and seventh panels) the parallel component of the wave magnetic field and the ion and magnetic pressures in the Pi2 frequency range, (eighth panel) the ion (proton) velocities perpendicular and parallel to the magnetic field, and (bottom six panels) proton and electron spectrograms for medium and low energies at 0°, 90°, and 180° (±30°) pitch angles obtained by the ERG spacecraft. The vertical lines indicate the times of the troughs of the parallel magnetic field component of the Pi2 wave (sixth panel).

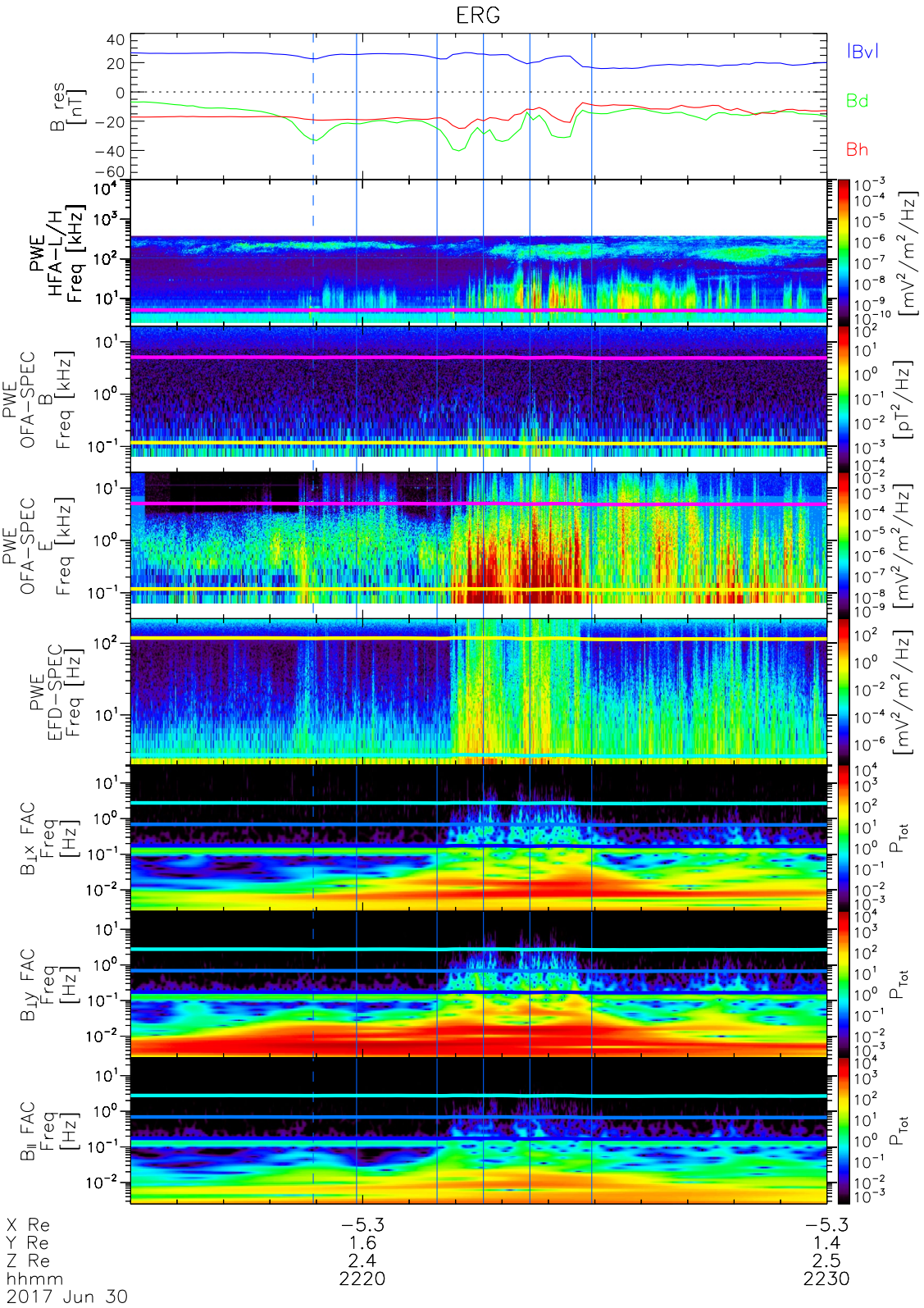

Figure 4.

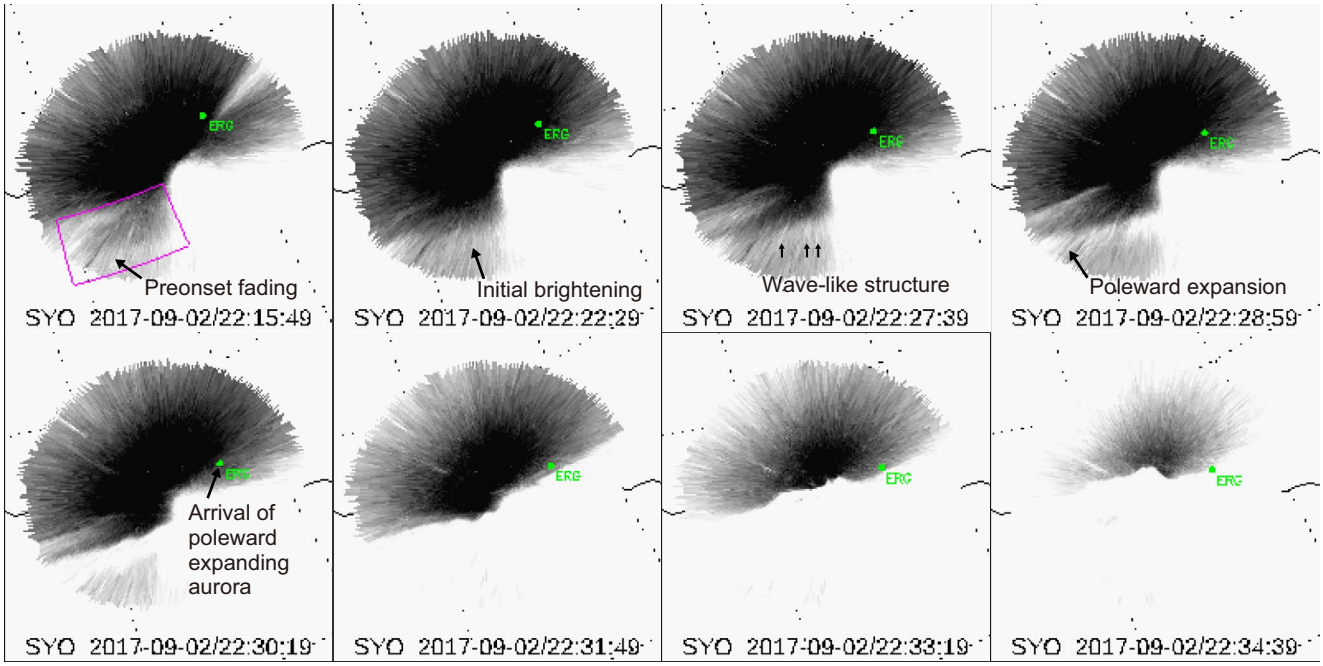

Figure 5. Auroral snapshots of the onset arc development from Syowa for the September 2, 2017 event. The black-white scale ranges from 180 to 255. The large black arrows indicate approximate locations of the beginnings of the auroral steps. Auroral count variations in the magenta box in the 22:15:49 UT image are shown in Figure S5. See Movie S2 for the full sequence.

plasma sheet thinning from ~22:13 to ~22:31 UT. Dipolarization (increase in the residual northward B_h) began with ~1 min period and more rapid oscillations due to intense Pi2 and Pi1 pulsations (the fifth panel), respectively, at 22:31 UT, when the poleward-expanding aurora reached ERG's footprint. Since ERG's footprint was located poleward of the auroral onset arc (Figure 5), ERG observed outward expansion of the dipolarization region. At 22:35 UT, the residual earthward $|B_v|$ (Figure 6, the top panel) decreased, and higher-energy proton and electron fluxes and hence the ion pressure (the second panel from the bottom) largely enhanced, compared to the presubstorm level, indicating plasma sheet expansion and particle acceleration. The ion β (the bottom panel) was low, ~0.01–0.04, after 22:36 UT. Dipolarization ended at ~22:44 UT. Auroral kilometric radiation at ~100–300 kHz was seen at and before initial auroral brightening, and more intense radiation at and below this frequency occurred at poleward expansion (the fourth panel). This two-step development is consistent with Morioka et al. (2010, 2014). Intense electrostatic waves near the electron cyclotron frequency were also seen in the plasma sheet during dipolarization. Note again that the intense broadband noises between 22:53 and 23:00 UT were artificial signals caused by PWE calibration.

During dipolarization, ERG observed the same particle and wave features as the first event shown above. As shown in Figure 7, the magnetic field oscillated alternately between dipole-like and taillike configuration at ~1 min period (the third and fifth panels), with dipole-like configuration nearly at Pi2 wave troughs (the sixth panel, the vertical lines). The eastward magnetic field B_d (the fourth panel) tended to oscillate in phase with the Pi2 waves in the outer plasma sheet or plasma sheet boundary layer before ~22:35 UT and then out of phase in the inner plasma sheet, possibly related to field-aligned currents. In addition, some B_d peaks and troughs were seen between the Pi2 peak and trough (Figure S8). In the plasma sheet after 22:35 UT, energetic proton and electron fluxes with a few to tens of kiloelectronvolts (Figure 7, the bottom six panels) enhanced near dipole-like configuration and Pi2 wave troughs. The ion and magnetic pressures in the Pi2 frequency range (the seventh panel) were comparable and out of phase, indicating that magnetosonic

Figure 4. Exploration of energization and Radiation in Geospace (ERG) magnetic field and wave data from 22:15 to 22:30 UT on June 30, 2017. Shown are (top) the residual magnetic field, (second to fifth panels) electric and magnetic field power spectrograms at high frequencies, and (bottom three panels) wavelet scalograms for the two perpendicular and parallel components of the wave magnetic field at low frequencies. The magenta, yellow, cyan, light blue, and blue lines in the spectrograms and scalograms indicate the electron cyclotron, lower-hybrid, proton cyclotron, helium cyclotron, and oxygen cyclotron frequencies, respectively. The vertical lines indicate the times of the troughs of the parallel magnetic field component of the Pi2 wave shown in Figure 3.

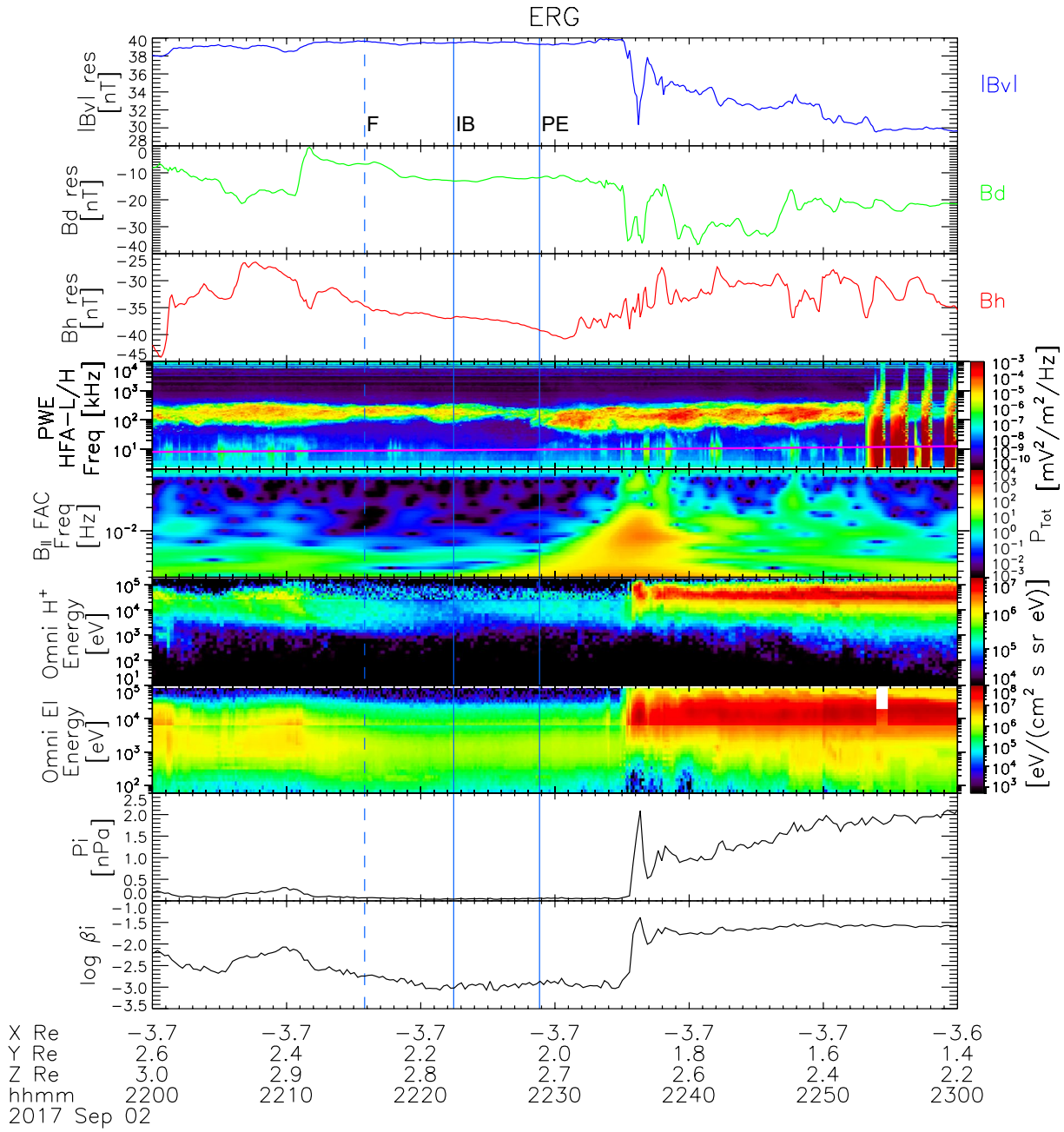

Figure 6. Exploration of energization and Radiation in Geospace (ERG) magnetic field, wave, and particle data from 22:00 to 23:00 UT on September 2, 2017 in the same format as Figure 2. The dashed vertical line indicates the beginning of preonset auroral fading (F). The solid vertical lines from the left indicate the beginnings of initial auroral brightening (IB) and poleward expansion (PE).

waves were in slow mode. The antiparallel (outward) low-energy proton flux and parallel and antiparallel low-energy electron fluxes appeared intermittently as well. The ion flow (the eighth panel) was slow at the beginning of dipolarization and then oscillated during dipolarization. As shown in Figure 8, intense Pi1 pulsations (the bottom three panels), electromagnetic waves below the electron cyclotron frequency (the third to fifth panels), and electrostatic waves near the electron cyclotron frequency (the second panel), if not all, tended to appear at the Pi2 wave troughs during dipolarization.

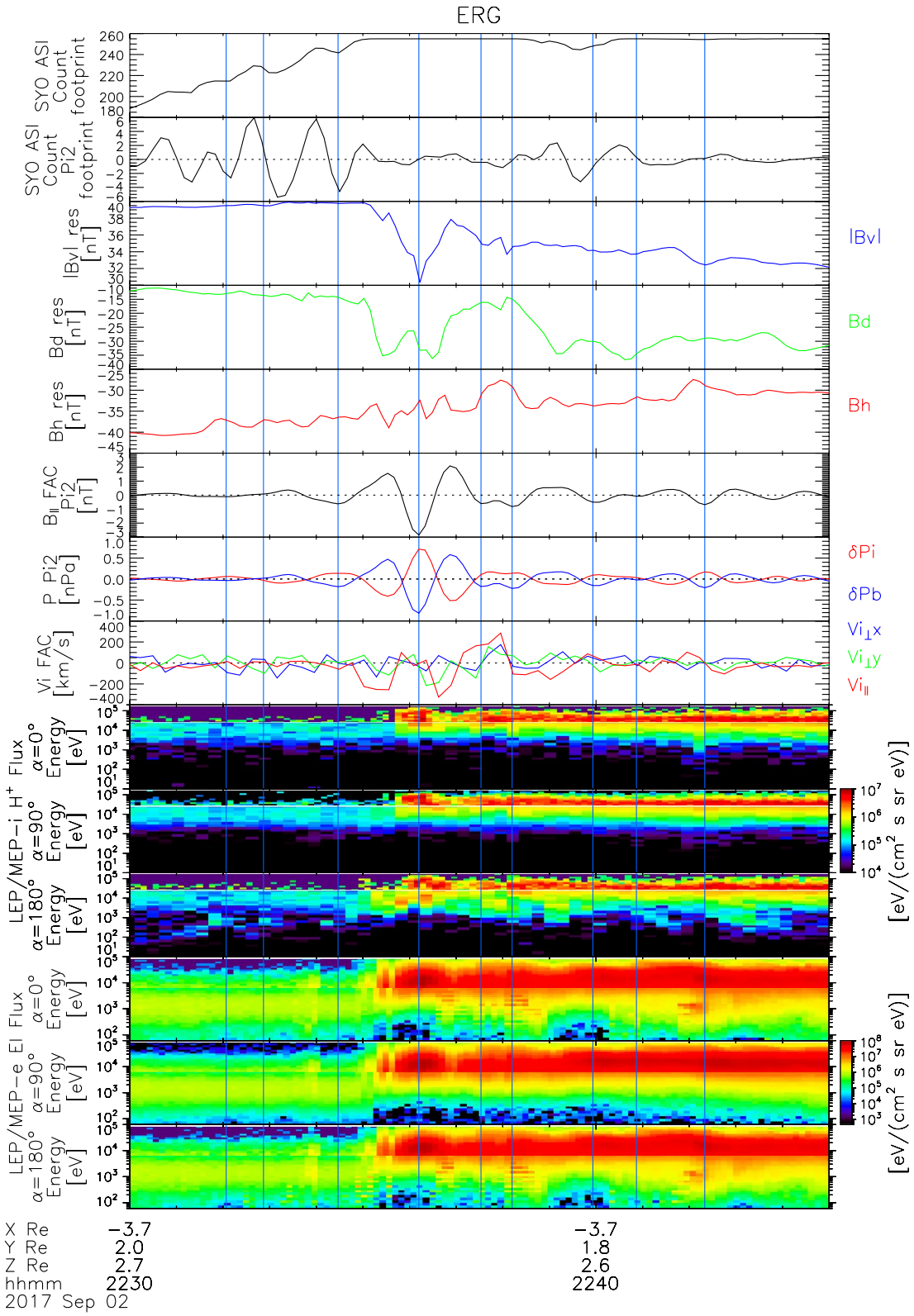

Figure 7. Auroral count at Exploration of energization and Radiation in Geospace's (ERG) footprint, and ERG magnetic field, wave, and particle data from 22:30 to 22:45 UT on September 2, 2017 in the same format as Figure 3. The vertical lines indicate the times of the troughs of the parallel magnetic field component of the Pi2 wave. Note that the auroral count was saturated (flat) after ~22:35 UT.

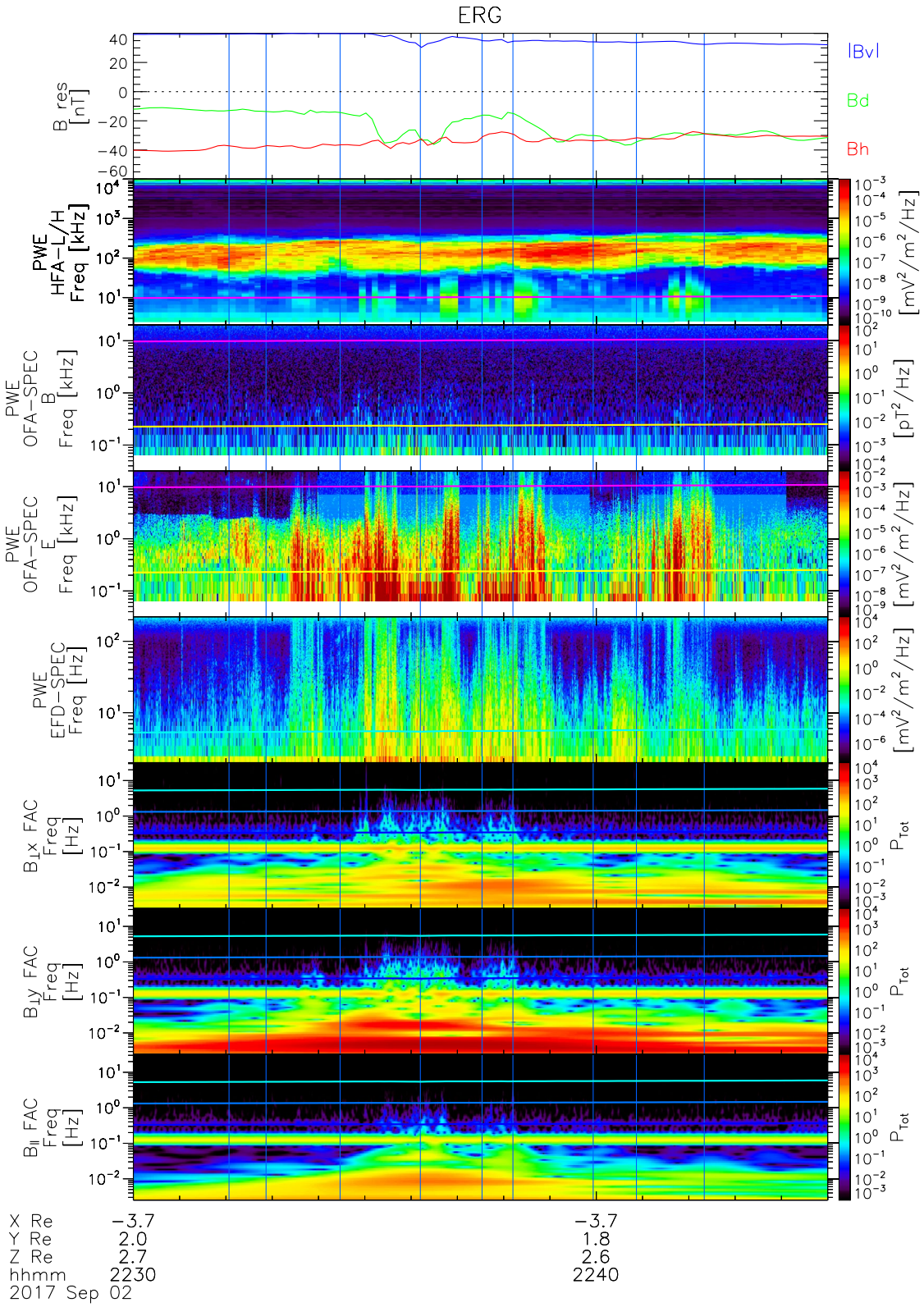

Figure 8. Exploration of energization and Radiation in Geospace (ERG) magnetic field and wave data from 22:30 to 22:45 UT on September 2, 2017 in the same format as Figure 4. The vertical lines indicate the times of the troughs of the parallel magnetic field component of the Pi2 wave shown in Figure 7.

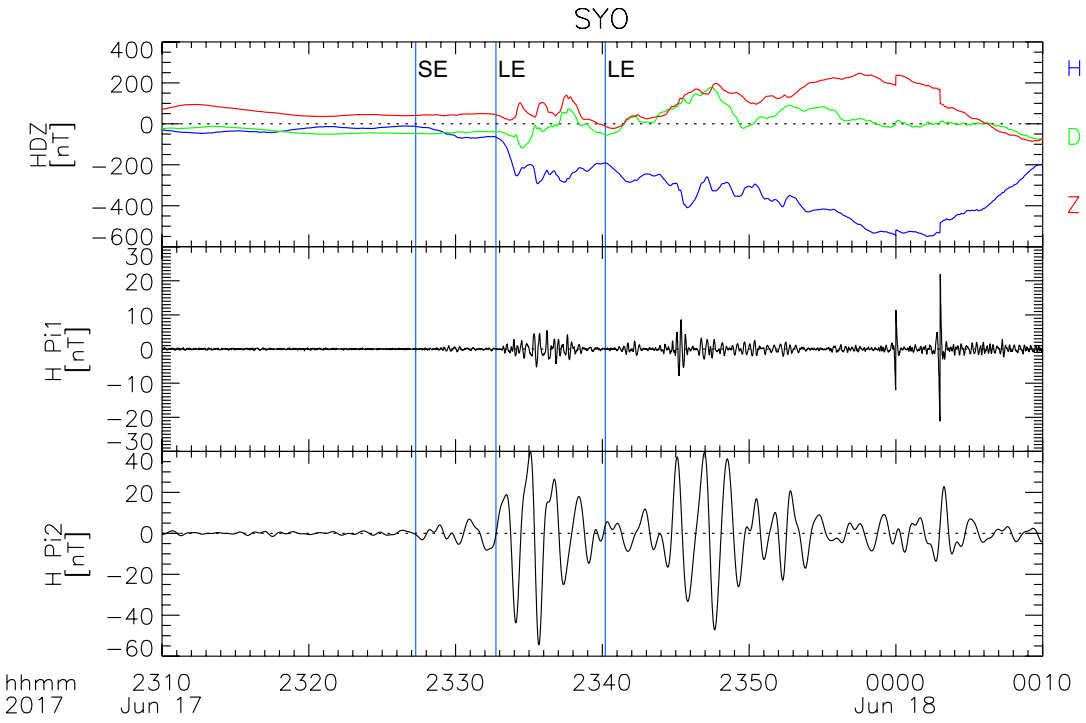

Figure 9. Ground magnetic field and Pi1 and Pi2 pulsations of the H component obtained by the fluxgate magnetometer at Syowa for the June 17, 2017 event. The vertical lines from the left indicate the beginnings of small (SE) and two large (LE) negative excursions of the H component, which possibly correspond to initial auroral brightening and poleward expansion, respectively.

2.3. The June 17, 2017 Event

Because auroral data from Syowa were unavailable for this event, we checked ground magnetic field data from Syowa instead. Syowa was located less than 1 h (in MLT) westward of ERG's footprint. As shown in Figure 9, a small negative excursion of the H component began at 23:27:17 UT, accompanied by a low-frequency portion of small-amplitude Pi2 pulsation. A large negative excursion then began at 23:32:45 UT, reaching ~−300 nT and accompanied by Pi1 pulsation and a high-frequency portion of large-amplitude Pi2 pulsation. According to Morioka et al. (2010, 2014), the small and subsequent large negative excursions possibly correspond to initial auroral brightening and auroral poleward expansion, respectively. Subsequently, the second large excursion of the H component began at 23:40:12 UT, reaching –500 nT and accompanied by another large-amplitude Pi2 pulsation and small-amplitude Pi1 pulsation. This excursion may correspond to the second auroral poleward expansion.

In this event ERG was outside the plasmasphere (Figure S9) and in the outer plasma sheet at $R \sim 5.1\ R_E$ until ~7 min after the second large geomagnetic excursion (Figure 10, the sixth and seventh panels). High-energy proton and electron fluxes and the residual northward B_h (the third panel) decreased and the residual earthward $|B_v|$ (the top panel) increased after ~23:30 UT, due to plasma sheet thinning. Dipolarization (increase in the residual northward B_h and decrease in the residual $|B_v|$) began with ~1 min period and more rapid oscillations due to intense Pi2 and Pi1 pulsations (the fifth panel), respectively, at ~23:47 UT, ~7 min after the second large geomagnetic excursion. Simultaneously, high-energy proton and electron fluxes and the ion pressure (the second panel from the bottom) largely enhanced, indicating plasma sheet expansion and particle acceleration. The ion β (the bottom panel) was ~0.02–0.03 during dipolarization. Dipolarization ended at ~23:59 UT. For this event, since we could not determine the relative location of ERG's footprint to the auroral onset arc, we could not determine the expansion direction of the dipolarization region at ERG. Auroral kilometric radiation at ~100–300 kHz occurred after the small geomagnetic excursion, and more intense radiation at and below this frequency occurred after each of the two large geomagnetic excursions

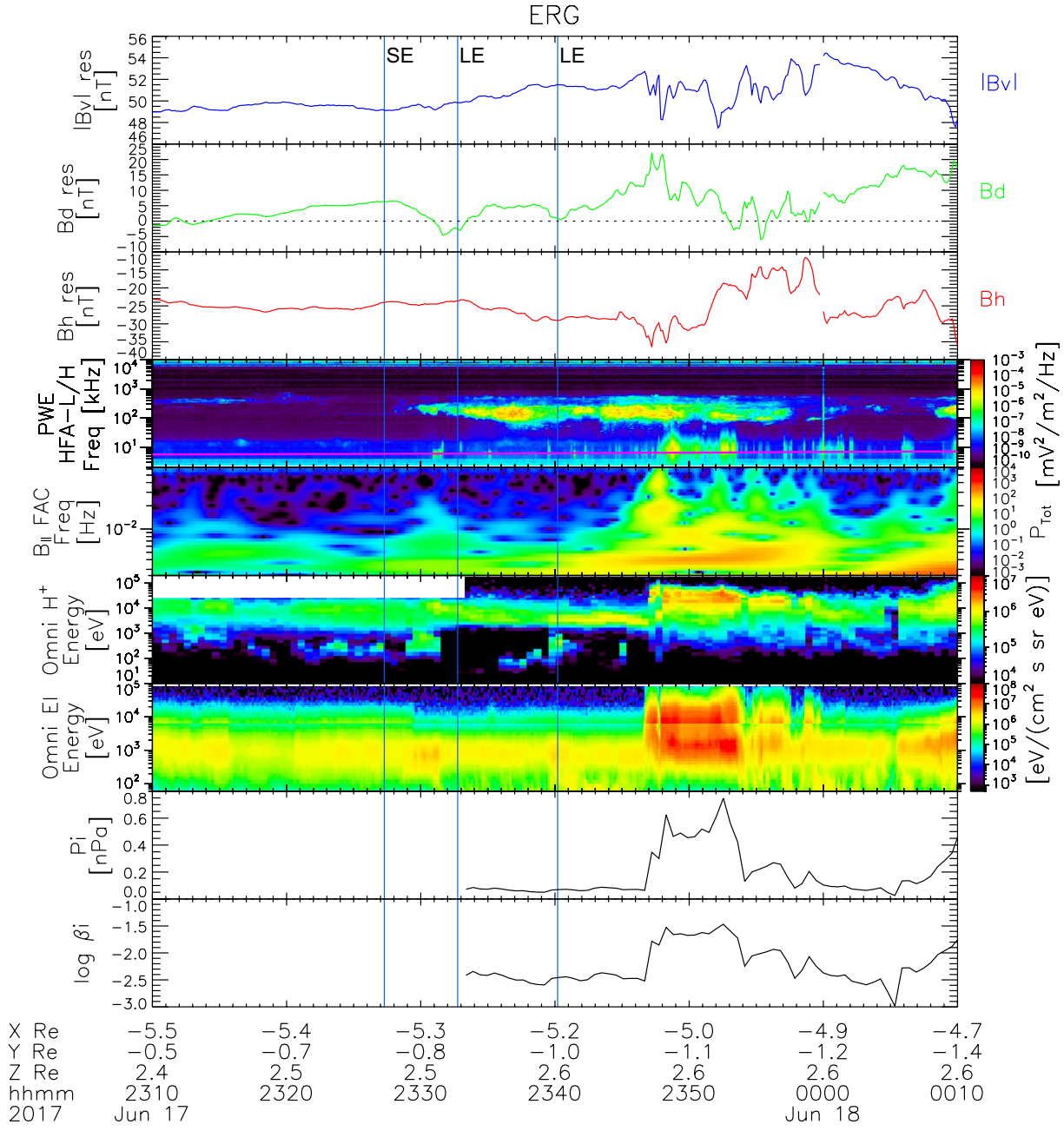

Figure 10. Exploration of energization and Radiation in Geospace (ERG) magnetic field, wave, and particle data from 23:10 UT on June 17, 2017 to 00:10 UT on June 18, 2017 in the same format as Figure 2. The vertical lines from the left indicate the beginnings of small (SE) and two large (LE) negative excursions of the H component of the ground magnetic field shown in Figure 9.

(the fourth panel). Intense electrostatic waves near the electron cyclotron frequency were also seen in the plasma sheet during dipolarization.

Particle and wave features similar to the other events can be seen during dipolarization in this event (Figures 11 and 12). Both residual B_h and $|B_v|$ decreased at ~23:47 UT (the dashed vertical line), possibly related to the explosive growth phase. After that, ERG observed alternate magnetic field oscillation between dipole-like and taillike configuration at ~1 min period, B_d oscillation (see also Figure S10), enhancements of energetic proton and electron fluxes with a few to tens of kiloelectronvolts, and tendency of appearance of intense Pi1, electromagnetic, and electrostatic waves near dipole-like configuration and Pi2 wave troughs (the vertical lines). Note that the ion and magnetic pressures in the Pi2 frequency range (Figure 11, the fifth

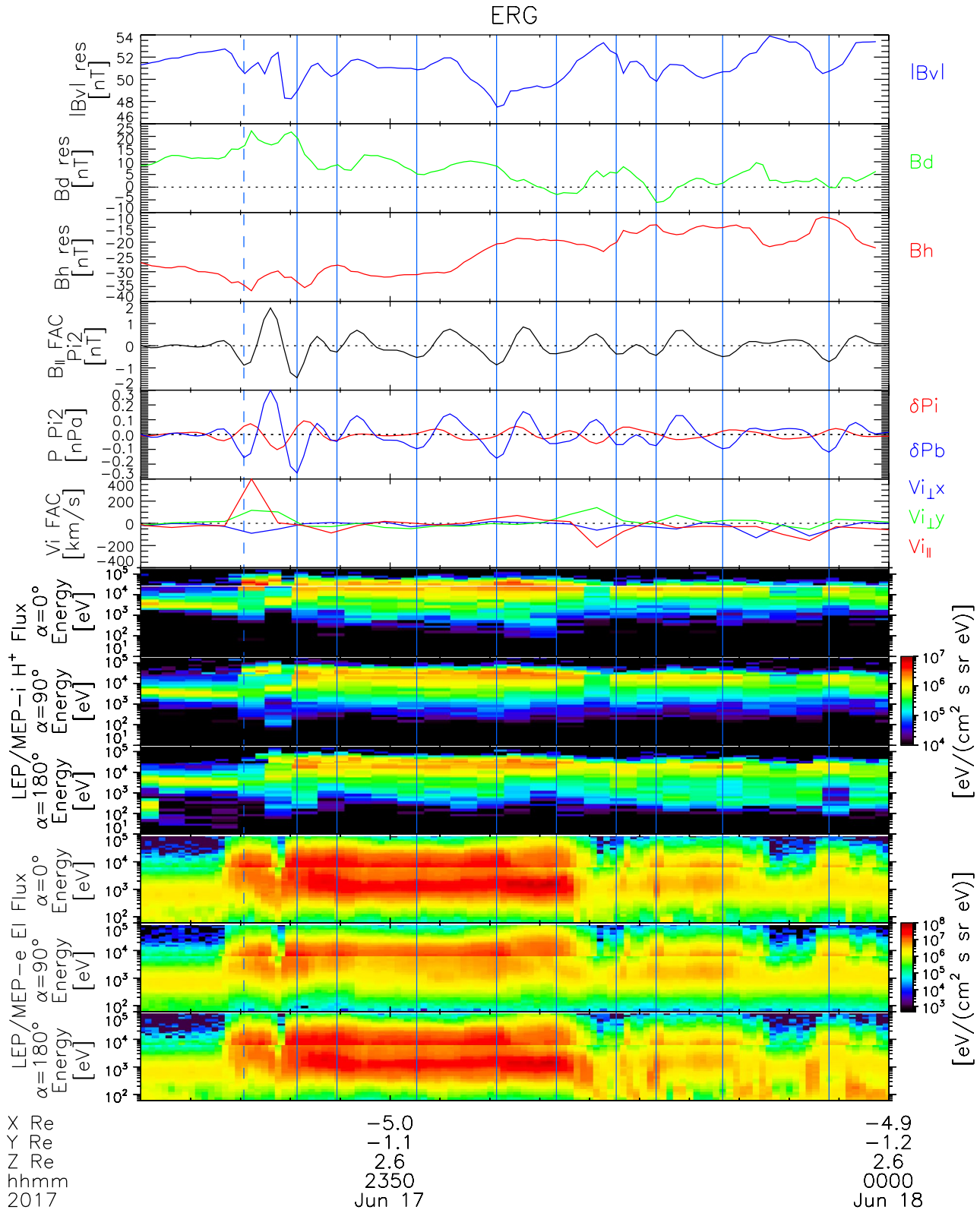

Figure 11. Exploration of energization and Radiation in Geospace (ERG) magnetic field, wave, and particle data from 23:45 UT on June 17, 2017 to 00:00 UT on June 18, 2017 in the same format as Figure 3. The vertical lines indicate the times of the troughs of the parallel magnetic field component of the Pi2 wave.

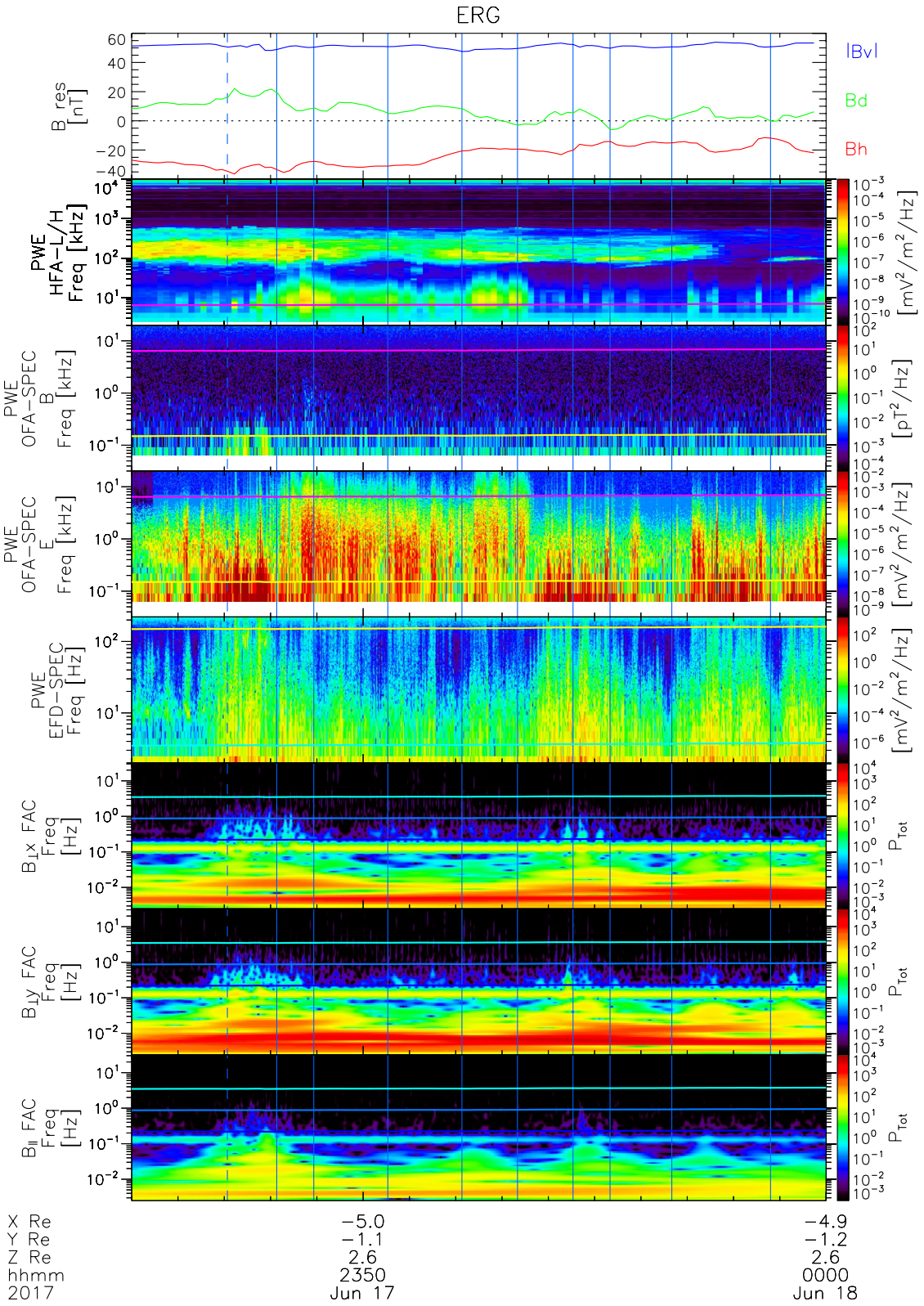

Figure 12. Exploration of energization and Radiation in Geospace (ERG) magnetic field and wave data from 23:45 UT on June 17, 2017 to 00:00 UT on June 18, 2017 in the same format as Figure 4. The vertical lines indicate the times of the troughs of the parallel magnetic field component of the Pi2 wave shown in Figure 11.

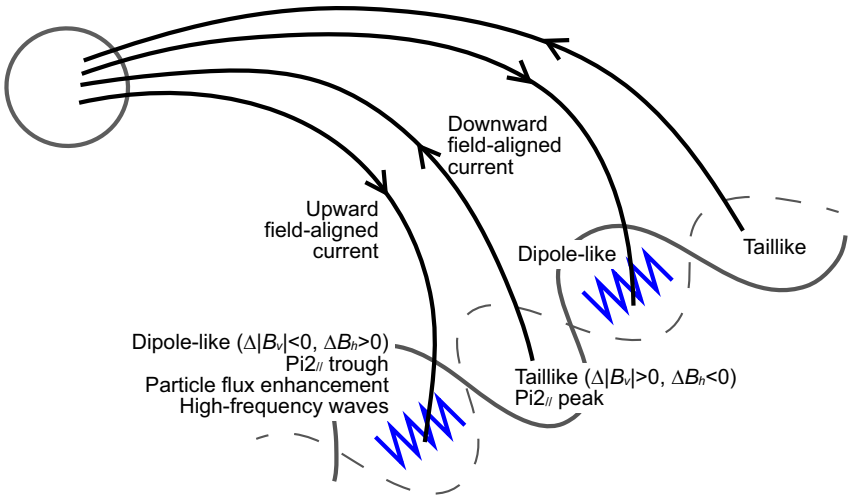

Figure 13. Schematic illustrating the observed features of the dipole-like and taillike configuration regions. The field-aligned currents in between are omitted. See text for details.

panel) were not always out of phase during this interval. They were even in phase sometimes, for example, at ~23:49 UT. Fast and slow modes may have been mixed during this interval, which is possibly why several peaks and troughs of B_h and $|B_v|$ did not necessarily occur exactly at the same time as those of the Pi2 waves. Furthermore, the ion and magnetic pressure perturbations were not comparable nearly throughout the interval. Since the ion pressure was low near the plasma sheet boundary at ERG, slow mode waves were possibly difficult to exist there. At the dipolarization onset, the parallel ion flow was directed inward, while the perpendicular flow was westward.

3. Discussion

Using ERG spacecraft data, we studied magnetic field and energetic particle flux oscillations in the Pi2 frequency range and high-frequency waves deep in the inner magnetosphere at $R \sim 4$–$5\ R_E$ during substorm dipolarization for three events. The magnetic field oscillated alternately between dipole-like and tail-like configuration at ~1 min period during dipolarization. When the magnetic field was dipole-like, the parallel component of the Pi2 waves was at trough. Both energetic ion and electron fluxes with a few to tens of kiloelectronvolts enhanced out of phase, indicating that magnetosonic waves were in slow mode. Field-aligned currents also oscillated. In addition, we found that broadband waves from the Pi1 frequency range to above the electron cyclotron frequency tended to appear in the central plasma sheet near dipole-like configuration. A schematic of these results is presented in Figure 13. Note that our events are related to near-Earth large-scale dipolarization, different from the "dipolarization front" (Nakamura et al., 2002; Runov et al., 2009) or reconnection jet front, for which Yang et al. (2017) showed high-frequency electrostatic waves near and above the electron cyclotron frequency in a tailward region.

In the present events dipolarization occurred deep in the inner magnetosphere (inside geosynchronous orbit) when the expanding aurora reached ERG's footprint during the substorm expansion phase. Irrespective of the expansion direction of the dipolarization region, the observed ~1 min period oscillations are similar to previous observations reported as signatures of ballooning instability (e.g., Roux et al., 1991). Chang and Cheng (2015), Cheng and Lui (1998), and Saito et al. (2008) suggested that ballooning instability occurs under high β ($\gg$1) in the near-Earth magnetotail, but in the present events β was very low, ~0.01–0.06, away from the magnetic equator deep in the inner magnetosphere (Figures 2, 6, and 10). Hence it is possible that ballooning instability occurred at the high-β equator, while ERG observed the effects of equatorial oscillations away from the equatorial source region.

In addition, while Cheng and Lui (1998) and Saito et al. (2008), and more recent studies with THEMIS data (e.g., Chang & Cheng, 2015; Kalmoni et al., 2015; Park et al., 2010; Xing et al., 2013) analyzed dipolarization events observed beyond geosynchronous orbit, some others analyzed those observed at and near (even

inside) geosynchronous orbit, where the background northward dipole field as well as the radial field is larger (e.g., Erickson et al., 2000; Pu et al., 1997, 1999; Roux et al., 1991). Although plasma and magnetic conditions differ between near and beyond geosynchronous orbit, the growth of ballooning instability is determined from the balance between the pressure and magnetic gradient forces and the curvature force of stretched field lines. The northward magnetic field may not necessarily be very small initially, but how far magnetic field lines become stretched is important as a condition for the instability. In fact, ERG observed the signatures of field line stretching, that is, B_h decrease, $|B_v|$ increase, and plasma sheet thinning before dipolarization onsets in the present events (Figures 2, 6, and 10).

Ballooning instability, which can grow under the pressure gradient, is thought to trigger current disruption and dipolarization. Once ballooning instability grows sufficiently in a localized current disruption/dipolarization onset region, the resulting increase in the pressure gradient may promote the same process on the outward side. Repeating this process may correspond to outward expansion of the dipolarization region and hence auroral poleward expansion associated with substorms. The outward expansion speed of the dipolarization region is typically ~200–300 km/s or ~2–3 R_E/min (Jacquey et al., 1991; Ohtani et al., 1992a). On the inward side of the onset region, the pressure gradient presumably does not change very much or even decreases, suppressing ballooning instability. That is, inward expansion of the dipolarization region and auroral equatorward expansion may usually be less explosive than outward/poleward expansion. The inward expansion speed of the dipolarization region is typically ~50 km/s or ~0.5 R_E/min (Ohtani et al., 2018).

The June 30, 2017 event, however, may be unusual. ERG's footprint was equatorward of the auroral onset arc, that is, ERG was located inward of the dipolarization onset region. According to mapping with the T96 model, the auroral onset arc and the ERG location roughly correspond to $X \sim -10$ and $-7.8\ R_E$, respectively, at the equatorial plane of the magnetosphere at the beginning of auroral equatorward expansion. Since auroral equatorward expansion took ~1.5 min between these positions, the inward expansion speed of the dipolarization region is estimated at ~160 km/s or ~1.5 R_E/min, which is ~3 times higher than usual. Another unusual feature is that inward expansion began suddenly. Some magnetospheric and ionospheric conditions possibly changed largely just before aurora equatorward expansion. A possible factor may be the westward flow observed by ERG before auroral equatorward expansion and dipolarization (Figure 3, the eighth panel). This flow may correspond to subauroral polarization streams (SAPS), resulting in shear flow ballooning instability (cf. Henderson et al., 2018).

For another possible interpretation of the Pi2 waves, Liu et al. (2017) and Wang et al. (2020) discussed earthward-propagating Pi2 waves generated by magnetic reconnection or reconnection jet fronts (or dipolarizing flux bundles, DFBs). Since such waves propagate across the magnetic field, they should be in fast mode, not in slow mode. In Liu et al.'s (2017) event, the THEMIS P5 spacecraft observations are similar to our events, because fast earthward flows were not seen away from the DFBs outside the plasmasphere at the beginning of dipolarization (net B_z increase). Here note that slow, weak dipolarization occurred there in their event as well, although they do not seem to have mentioned it in their paper. They showed out-of-phase plasma and magnetic pressure perturbations during dipolarization. Although such perturbations are usually regarded as being in slow mode and fast mode waves should be evidenced by in-phase pressure perturbations, Liu et al. (2017) attributed the observed perturbations to vertical motion of the plasma sheet, suggesting from the large Poynting flux perpendicular to the background magnetic field that fast mode waves were dominant. For our dipolarization events, $V_{i\perp x}$ (Figures 3, 7, and 11), which was nearly in the $-Z$ direction in SM coordinates, oscillated, but did not necessarily change its direction alternately, inconsistent with up and down motion of the plasma sheet. Hence, we can conclude that the observed waves accompanied by out-of-phase pressure perturbations were in slow mode or at least contained slow mode, if not pure, which are unlikely to have been generated by a fast earthward flow from the reconnection site.

Tuner et al. (2015) suggested that energetic particle injection deep in the inner magnetosphere is limited up to 250 keV in contrast to that at higher L, resulting from interaction with a fast magnetosonic wave in the Pi2 frequency range unlike injection at higher L. The region and mode of Pi2 waves differ between Turner et al. (2015) and our events, however. Turner et al. (2015) Pi2 waves were observed inside the plasmasphere and were in fast mode. On the other hand, our Pi2 waves were observed outside the plasmasphere (Figures S3, S7, and S9) for the three events and were mainly in slow mode for the first and second events (Figures 3 and 7) and at least contained slow mode for the third event near the plasma sheet

boundary (Figure 11). Our observations are similar to those at larger distances, as mentioned above. Hence the mechanism of dipolarization and particle injection most likely differs between inside and outside the plasmasphere.

The eastward magnetic field B_d oscillated during dipolarization (Figures 3, 7, and 11). In dipole-like configuration (the vertical lines), B_d tended to deviate westward in the outer plasma sheet and eastward in the inner plasma sheet. On the other hand, in taillike configuration (between the vertical lines), the deviations tended to be in the opposite directions. If these alternate changes were generated by field-aligned currents, the field-aligned currents were possibly located somewhere between the outer and inner plasma sheet and changed its direction alternately, upward in dipole-like configuration and downward in taillike configuration, as depicted in Figure 13. This tendency can be confirmed in Figures S4, S8, and S10, where the solid and dashed magenta lines can be regarded as corresponding to upward and downward field-aligned currents, respectively. The alternate field-aligned currents were inferred from ionospheric shear flows by Hosokawa et al. (2013), who suggested that upward field-aligned currents correspond to auroral wave-like structure. Similar correspondence seems to be the case with the June 30, 2017 event shown here. That is, most Pi2 troughs (Figure 3, the first, second, fourth, and fifth solid lines) coincided with enhancement of the auroral luminosity at ERG's footprint; the large enhancement at ~22:21 UT may be related to slight increase in the residual B_h. (For the September 2, 2017 event, such correspondence is difficult to see because of saturation of the auroral count.) Roux et al. (1991) also inferred alternate field-aligned currents from magnetospheric observations, but they suggested that because of ion and electron separation in westward-propagating ballooning waves, the resulting upward and downward field-aligned currents be seen alternately during taillike-then-dipole-like (Pi2 peak-then-trough) changes and during dipole-like-then-taillike (Pi2 trough-then-peak) changes, respectively. Such field-aligned currents can be seen in some cases in Figures S4, S8, and S10 (but are omitted in the schematic of Figure 13). Thus, it is likely that the field-aligned currents are generated not only between the dipole-like and taillike configuration regions, as expected from the ballooning instability theory, but also in the dipole-like and taillike regions. The upward field-aligned currents in dipole-like configuration are possibly generated by electron acceleration discussed below.

From observations of the wavelength of wave-like auroral structure, the scale size of a field-aligned current pair can be regarded as ~1–3° in magnetic longitude or ~100–200 km in the ionosphere, which corresponds to ~1,000–3,000 km in the magnetic equator (Chang & Cheng, 2015; Liang et al., 2008). Saito et al. (2008) also obtained similar results of the wavelength of ballooning waves from magnetotail observations. If Saito et al. (2008) method can be applied to the interval from the first trough of the Pi2 wave to the beginning of dipolarization (net B_z increase) for our June 30 and 17, 2017 events, the wavelength was estimated at ~3,000 km, taking the wave period as 60 s and the azimuthal velocity fluctuation $\delta V_{\perp} y$ as 50 km/s. These scales are smaller than that of the wedgelet that consists of the field-aligned current pair located at the western and eastern flanks of an equatorward-moving streamer in the ionosphere (the western flank corresponds to the auroral streamer), ~600 km, and the corresponding fast earthward flow in the magnetotail, ~2–3 R_E (Nishimura et al., 2020).

We showed that high-frequency waves in a wide range from the Pi1 range to above the electron cyclotron frequency tended to appear in the central plasma sheet intermittently, accompanied by energetic ion and electron fluxes, when magnetic field configuration was dipole-like during dipolarization-associated oscillation. The high-frequency waves are possibly related to the cross-field current instability (Lui et al., 1991). Ohtani et al. (2002) showed that electrons were energized near the neutral sheet during dipolarization similarly to the present events, suggesting that this can be explained by the ion Weibel and modified two-stream instabilities. Note that other acceleration mechanisms, such as Fermi acceleration (Yao et al., 2017), may also work in dipole-like configuration.

Meanwhile, the high-frequency waves may be excited by coupling with enhanced ballooning instability (Cheng, 2004; Cheng & Lui, 1998). Alternatively, the opposite may be a possibility or the association may be just coincidental (Lui, 2020). In any case, the observed intermittency of the high-frequency waves may indicate current filamentation associated with the cross-field current instability (Lui, 2004), which causes field-aligned electron acceleration (upward field-aligned current) and possibly periodic auroral brightening during auroral poleward expansion/breakup. The high-frequency waves in dipole-like configuration seem

to coincide with enhancement of the auroral luminosity at ERG's footprint, but more details need further investigation to conclude definitely.

Data Availability Statement

ERG spacecraft data sets for this study are available in these in-text data citation references: Asamura, Miyoshi, and Shinohara (2018), Kasahara et al. (2018a, 2018d, 2018e, 2019, 2021), Matsuokaet al. (2018a, 2018b), Miyoshi et al. (2018b), Wang et al. (2018), and Yokota et al. (2018). The Syowa all-sky imager and magnetic field data were provided by National Institute of Polar Research, Japan (http://iugonet0.nipr.ac.jp/data/ and http://polaris.nipr.ac.jp/~aurora/icam/). OMNI solar wind data and the *Sym-H* index used for calculation of ERG's footprints are available at NASA CDAWeb (King & Papitashvili, 2005; https://cdaweb.gsfc.nasa.gov/pub/data/omni/omni_cdaweb/hro_1min/). Data access and processing were done using the Space Physics Environment Data Analysis System (SPEDAS) version 4.1 (Angelopoulos et al., 2019; http://spedas.org/wiki/index.phptitle=Downloads_and_Installation) and ERG plug-in tool version 8.13.

Acknowledgments
This work was in part carried out by a joint research program of Institute for Space-Earth Environmental Research, Nagoya University, and was in part supported by a Grant-in-Aid for Scientific Research of Japan Society for the Promotion of Science (20H01957 Scientific Research B). The ERG Science Center (Miyoshi et al., 2018a; https://ergsc.isee.nagoya-u.ac.jp/) was operated by Institute of Space and Astronautical Science, Japan Aerospace Exploration Agency, and Institute for Space-Earth Environmental Research, Nagoya University. Auroral Observation at Syowa Station and the Upper Atmosphere Physics Monitoring Observation at Syowa Station were mainly supported by the Research Program of Japanese Antarctic Research Expedition (JARE) of the Ministry of Education, Culture, Sports, Science, and Technology of Japan (MEXT). The distribution of the Syowa data was partly supported by the Inter-university Upper atmosphere Global Observation NETwork (IUGONET) project (http://www.iugonet.org/) funded by the MEXT. We thank J. H. King and N. E. Papitashvili for the OMNI solar wind data and the *Sym-H* index. The *Sym-H* index is originally produced and distributed by World Data Center for Geomagnetism, Kyoto (http://wdc.kugi.kyoto-u.ac.jp/aeasy/index.html).

References

Alken, P., Thébault, E., Beggan, C. D., Amit, H., Aubert, J., Baerenzung, J., et al. (2021). International geomagnetic reference field: The thirteenth generation. *Earth Planets and Space*, *73*, 49. https://doi.org/10.1186/s40623-020-01288-x

Angelopoulos, V., Cruce, P., Drozdov, A., Grimes, E. W., Hatzigeorgiu, N., King, D. A., et al. (2019). The Space Physics Environment Data Analysis System (SPEDAS). *Space Science Reviews*, *215*, 9. https://doi.org/10.1007/s11214-018-0576-4

Asamura, K., Kazama, Y., Yokota, S., Kasahara, S., & Miyoshi, Y. (2018). Low-energy particle experiments-ion mass analyzer (LEPi) onboard the ERG (Arase) satellite. *Earth Planets and Space*, *70*, 70. https://doi.org/10.1186/s40623-018-0846-0

Asamura, K., Miyoshi, Y., & Shinohara, I. (2018). *The LEPi instrument Level-2 3D flux data of Exploration of energization and Radiation in Geospace (ERG) Arase satellite, Version v03_00*. ERG Science Center, Institute for Space-Earth Environmental Research, Nagoya University. https://doi.org/10.34515/DATA.ERG-05000

Baker, D. N., Pulkkinen, T. I., Angelopoulos, V., Baumjohann, W., & McPherron, R. L. (1996). Neutral line model of substorms: Past results and present view. *Journal of Geophysical Research: Space Physics*, *101*(A6), 975–13010. https://doi.org/10.1029/95JA03753

Bhattacharjee, A., Ma, Z. W., & Wang, X. (1998). Ballooning instability of a thin current sheet in the high-Lundquist-number magnetotail. *Geophysical Research Letters*, *25*(6), 861–864. https://doi.org/10.1029/98GL00412

Chang, T.-F., & Cheng, C.-Z. (2015). Relationship between wave-like auroral arcs and Pi2 disturbances in plasma sheet prior to substorm onset. *Earth Planets and Space*, *67*, 168. https://doi.org/10.1186/s40623-015-0334-8

Chen, L.-J., Bhattacharjee, A., Sigsbee, K., Parks, G., Fillingim, M., & Lin, R. (2003). Wind observations pertaining to current disruption and ballooning instability during substorms. *Geophysical Research Letters*, *30*(6), 1335. https://doi.org/10.1029/2002GL016317

Cheng, C. Z. (2004). Physics of substorm growth phase, onset, and dipolarization. *Space Science Reviews*, *113*(1–2), 207–270. https://doi.org/10.1023/B:SPAC.0000042943.59976.0e

Cheng, C. Z., & Lui, A. T. Y. (1998). Kinetic ballooning instability for substorm onset and current disruption observed by AMPTE/CCE. *Geophysical Research Letters*, *25*(21), 4091–4094. https://doi.org/10.1029/1998GL900093

Erickson, G. M., Maynard, N. C., Burke, W. J., Wilson, G. R., & Heinemann, M. A. (2000). Electromagnetics of substorm onsets in the near-geosynchronous plasma sheet. *Journal of Geophysical Research*, *105*(A11), 25290. https://doi.org/10.1029/1999JA000424

Henderson, M. G., Morley, S. K., & Kepko, L. E. (2018). SAPS-associated explosive brightening on the duskside: A new type of onset-like disturbance. *Journal of Geophysical Research: Space Physics*, *123*, 197–210. https://doi.org/10.1002/2017JA024472

Holter, Ø., Altman, C., Roux, A., Perraut, S., Pedersen, A., Pécseli, H., et al. (1995). Characterization of low frequency oscillations at substorm breakup. *Journal of Geophysical Research*, *100*(A10), 109119. https://doi.org/10.1029/95JA00990

Hosokawa, K., Milan, S. E., Lester, M., Kadokura, A., Sato, N., & Bjornsson, G. (2013). Large flow shears around auroral beads at substorm onset. *Geophysical Research Letters*, *40*, 4987–4991. https://doi.org/10.1002/grl.50958

Jacquey, C., Sauvaud, J. A., & Dandouras, J. (1991). Location and propagation of the magnetotail current disruption during substorm expansion: Analysis and simulation of an ISEE multi-onset event. *Geophysical Research Letters*, *18*(3), 389–392. https://doi.org/10.1029/90GL02789

Kalmoni, N. M. E., Rae, I. J., Watt, C. E. J., Murphy, K. R., Forsyth, C., & Owen, C. J. (2015). Statistical characterization of the growth and spatial scales of the substorm onset arc. *Journal of Geophysical Research: Space Physics*, *120*, 8503–8516. https://doi.org/10.1002/2015JA021470

Kasaba, Y., Ishisaka, K., Kasahara, Y., Imachi, T., Yagitani, S., Kojima, H., et al. (2017). Wire Probe Antenna (WPT) and Electric Field Detector (EFD) of Plasma Wave Experiment (PWE) aboard the Arase satellite: Specifications and initial evaluation results. *Earth Planets and Space*, *69*, 174. https://doi.org/10.1186/s40623-017-0760-x

Kasahara, S., Yokota, S., Hori, T., Keika, K., Miyoshi, Y., & Shinohara, I. (2018a). *The MEP-e instrument Level-2 3-D flux data of Exploration of energization and Radiation in Geospace (ERG) Arase satellite, Version v01_01*. ERG Science Center, Institute for Space-Earth Environmental Research, Nagoya University. https://doi.org/10.34515/DATA.ERG-02000

Kasahara, S., Yokota, S., Mitani, T., Asamura, K., Hirahara, M., Shibano, Y., & Takashima, T. (2018b). Medium-energy particle experiments–electron analyzer (MEP-e) for the exploration of energization and radiation in geospace (ERG) mission. *Earth Planets and Space*, *70*, 69. https://doi.org/10.1186/s40623-018-0847-z

Kasahara, Y., Kasaba, Y., Kojima, H., Yagitani, S., Ishisaka, K., Kumamoto, A., et al. (2018c). The Plasma Wave Experiment (PWE) on board the Arase (ERG) satellite. *Earth Planets and Space*, *70*, 86. https://doi.org/10.1186/s40623-018-0842-4

Kasahara, Y., Kasaba, Y., Matsuda, S., Shoji, M., Nakagawa, T., Ishisaka, K., et al. (2019). *The PWE/EFD instrument Level-2 electric field spectrum data of Exploration of energization and Radiation in Geospace (ERG) Arase satellite, Version v02_02*. ERG Science Center, Institute for Space-Earth Environmental Research, Nagoya University. https://doi.org/10.34515/DATA.ERG-07004

Kasahara, Y., Kojima, H., Matsuda, S., Ozaki, M., Yagitani, S., Shoji, M., et al. (2018d). *The PWE/OFA instrument Level-2 power spectrum data of Exploration of energization and Radiation in Geospace (ERG) Arase satellite, Version v02_01*. ERG Science Center, Institute for Space-Earth Environmental Research, Nagoya University. https://doi.org/10.34515/DATA.ERG-08000

Kasahara, Y., Kumamoto, A., Tsuchiya, F., Kojima, H., Matsuda, S., Matsuoka, A., et al. (2021). *The PWE/HFA instrument Level-3 electron density data of Exploration of energization and Radiation in Geospace (ERG) Arase satellite, Version, v01_02*. ERG Science Center, Institute for Space-Earth Environmental Research, Nagoya University. https://doi.org/10.34515/DATA.ERG-10001

Kasahara, Y., Kumamoto, A., Tsuchiya, F., Matsuda, S., Shoji, M., Nakamura, S., et al. (2018e). *The PWE/HFA instrument Level-2 spectrum data of Exploration of energization and Radiation in Geospace (ERG) Arase satellite, Version v01_02*. ERG Science Center, Institute for Space-Earth Environmental Research, Nagoya University. https://doi.org/10.34515/DATA.ERG-10000

Kazama, Y., Wang, B.-J., Wang, S.-Y., Ho, P. T. P., Tam, S. W. Y., Chang, T.-F., et al. (2017). Low-energy particle experiments-electron analyzer (LEPe) onboard the Arase spacecraft. *Earth Planets and Space*, *69*, 165. https://doi.org/10.1186/s40623-017-0748-6

Keiling, A., Angelopoulos, V., Larson, D., Lin, R., McFadden, J., Carlson, C., et al. (2008a). Correlation of substorm injections, auroral modulations, and ground Pi2. *Geophysical Research Letters*, *35*, L17S22. https://doi.org/10.1029/2008GL033969

Keiling, A., Angelopoulos, V., Larson, D., McFadden, J., Carlson, C., Fillingim, M., et al. (2008b). Multiple intensifications inside the auroral bulge and their association with plasma sheet activities. *Journal of Geophysical Research*, *113*, A12216. https://doi.org/10.1029/2008JA013383

King, J. H., & Papitashvili, N. E. (2005). Solar wind spatial scales in and comparisons of hourly Wind and ACE plasma and magnetic field data. *Journal of Geophysical Research*, *110*, A02104. https://doi.org/10.1029/2004JA010649

Kumamoto, A., Tsuchiya, F., Kasahara, Y., Kasaba, Y., Kojima, H., Yagitani, S., et al. (2018). High Frequency Analyzer (HFA) of Plasma Wave Experiment (PWE) onboard the Arase spacecraft. *Earth Planets and Space*, *70*, 82. https://doi.org/10.1186/s40623-018-0854-0

Lee, D.-Y., Kim, H.-S., Ohtani, S., & Park, M. Y. (2012). Statistical characteristics of plasma flows associated with magnetic dipolarizations in the near-tail region of. *Journal of Geophysical Research*, *117*, A01207. https://doi.org/10.1029/2011JA017246

Liang, J., Donovan, E. F., Liu, W. W., Jackel, B., Syrjäsuo, M., Mende, S. B., et al. (2008). Intensification of preexisting auroral arc at substorm expansion phase onset: Wave-like disruption during the first tens of seconds. *Geophysical Research Letters*, *35*, L17S19. https://doi.org/10.1029/2008GL033666

Liou, K., Meng, C.-I., Lui, A. T. Y., Newell, P. T., & Wing, S. (2002). Magnetic dipolarization with substorm expansion onset. *Journal of Geophysical Research*, *107*(A7), 1131. https://doi.org/10.1029/2001JA000179

Liu, J., Angelopoulos, V., Zhang, X.-J., Runov, A., Artemyev, A., Plaschke, F., et al. (2017). Ultralow frequency waves deep inside the inner magnetosphere driven by dipolarizing flux bundles. *Journal of Geophysical Research: Space Physics*, *122*, 10112–10128. https://doi.org/10.1002/2017JA024270

Lui, A. T. Y. (1996). Current disruption in the Earth's magnetosphere: Observations and models. *Journal of Geophysical Research*, *101*(A6), 13088. https://doi.org/10.1029/96JA00079

Lui, A. T. Y. (2004). Potential plasma instabilities for substorm expansion onsets. *Space Science Reviews*, *113*(1–2), 127–206. https://doi.org/10.1023/B:SPAC.0000042942.00362.4e

Lui, A. T. Y. (2020). Evaluation of the cross-field current instability as a substorm onset process with auroral bead properties. *Journal of Geophysical Research: Space Physics*, *125*, e2020JA027867. https://doi.org/10.1029/2020JA027867

Lui, A. T. Y., Chang, C.-L., Mankofsky, A., Wong, H.-K., & Winske, D. (1991). A cross-field current instability for substorm expansions. *Journal of Geophysical Research: Space Physics*, *96*(A7), 11401. https://doi.org/10.1029/91JA00892

Lyons, L. R., Voronkov, I. O., Donovan, E. F., & Zesta, E. (2002). Relation of substorm breakup arc to other growth-phase auroral arcs. *Journal of Geophysical Research*, *107*(A11), 1390. https://doi.org/10.1029/2002JA009317

Matsuda, S., Kasahara, Y., Kojima, H., Kasaba, Y., Yagitani, S., Ozaki, M., et al. (2018). Onboard software of Plasma Wave Experiment aboard Arase: Instrument management and signal processing of Waveform Capture/Onboard Frequency Analyzer. *Earth Planets and Space*, *70*, 75. https://doi.org/10.1186/s40623-018-0838-0

Matsuoka, A., Teramoto, M., Imajo, S., Kurita, S., Miyoshi, Y., & Shinohara, I. (2018a). *The MGF instrument Level-2 high-resolution magnetic field data of Exploration of energization and Radiation in Geospace (ERG) Arase satellite, Version v03.04*. ERG Science Center, Institute for Space-Earth Environmental Research, Nagoya University. https://doi.org/10.34515/DATA.ERG-06000

Matsuoka, A., Teramoto, M., Imajo, S., Kurita, S., Miyoshi, Y., & Shinohara, I. (2018b). *The MGF instrument Level-2 spin-averaged magnetic field data of Exploration of energization and Radiation in Geospace (ERG) Arase satellite, Version v03.04*. ERG Science Center, Institute for Space-Earth Environmental Research, Nagoya University. https://doi.org/10.34515/DATA.ERG-06001

Matsuoka, A., Teramoto, M., Nomura, R., Nosé, M., Fujimoto, A., Tanaka, Y., et al. (2018c). The ARASE (ERG) magnetic field investigation. *Earth Planets and Space*, *70*, 43. https://doi.org/10.1186/s40623-018-0800-1

Mende, S., Angelopoulos, V., Frey, H. U., Donovan, E., Jackel, B., Glassmeier, K.-H., et al. (2009). Timing and location of substorm onsets from THEMIS satellite and ground based observations. *Annales Geophysicae*, *27*(7), 2813–2830. https://doi.org/10.5194/angeo-27-2813-2009

Miyashita, Y., & Ieda, A. (2018). Revisiting substorm events with preonset aurora. *Annales Geophysicae*, *36*(5), 1419–1438. https://doi.org/10.5194/angeo-36-1419-2018

Miyashita, Y., Machida, S., Ieda, A., Nagata, D., Kamide, Y., Nosé, M., et al. (2010). Pressure changes associated with substorm dipolarization in the near-Earth plasma sheet. *Journal of Geophysical Research*, *115*, A12239. https://doi.org/10.1029/2010JA015608

Miyoshi, Y., Hori, T., Shoji, M., Teramoto, M., Chang, T. F., Segawa, T., et al. (2018a). The ERG Science Center. *Earth Planets and Space*, *70*, 96. https://doi.org/10.1186/s40623-018-0867-8

Miyoshi, Y., Shinohara, I., & Jun, C.-W. (2018b). *The level-2 orbit data of Exploration of energization and radiation in Geospace (ERG) Arase satellite, version v03*. ERG Science Center, Institute for Space-Earth Environmental Research, Nagoya University. https://doi.org/10.34515/DATA.ERG-12000

Miyoshi, Y., Shinohara, I., Takashima, T., Asamura, K., Higashio, N., Mitani, T., et al. (2018c). Geospace exploration project ERG. *Earth Planets and Space*, *70*, 101. https://doi.org/10.1186/s40623-018-0862-0

Morioka, A., Miyoshi, Y., Kasaba, Y., Sato, N., Kadokura, A., Misawa, H., et al. (2014). Substorm onset process: Ignition of auroral acceleration and related substorm phases. *Journal of Geophysical Research: Space Physics*, *119*, 1044–1059. https://doi.org/10.1002/2013JA019442

Morioka, A., Miyoshi, Y., Miyashita, Y., Kasaba, Y., Misawa, H., Tsuchiya, F., et al. (2010). Two-step evolution of auroral acceleration at substorm onset. *Journal of Geophysical Research*, *115*, A11213. https://doi.org/10.1029/2010JA015361

Nakamura, R., Baumjohann, W., Klecker, B., Bogdanova, Y., Balogh, A., Rème, H., et al. (2002). Motion of the dipolarization front during a flow burst event observed by Cluster. *Geophysical Research Letters*, *29*(20), 1942–1951. https://doi.org/10.1029/2002GL015763

Nakamura, R., Oguti, T., Yamamoto, T., & Kokubun, S. (1993). Equatorward and poleward expansion of the auroras during auroral substorms. *Journal of Geophysical Research: Space Physics*, *98*(A4), 5743–5759. https://doi.org/10.1029/92JA02230

Nishimura, Y., Lyons, L. R., Gabrielse, C., Weygand, J. M., Donovan, E. F., & Angelopoulos, V. (2020). Relative contributions of large-scale and wedgelet currents in the substorm current wedge. *Earth Planets and Space*, *72*, 106. https://doi.org/10.1186/s40623-020-01234-x

Nishimura, Y., Yang, J., Pritchett, P. L., Coroniti, F. V., Donovan, E. F., Lyons, L. R., et al. (2016). Statistical properties of substorm auroral onset beads/rays. *Journal of Geophysical Research: Space Physics*, *121*, 8661–8676. https://doi.org/10.1002/2016JA022801

Ohtani, S., Kokubun, S., & Russell, C. T. (1992a). Radial expansion of the tail current disruption during substorms: A new approach to the substorm onset region. *Journal of Geophysical Research: Space Physics*, *97*(A3), 3129–3136. https://doi.org/10.1029/91JA02470

Ohtani, S., Motoba, T., Gkioulidou, M., Takahashi, K., & Singer, H. J. (2018). Spatial development of the dipolarization region in the inner magnetosphere. *Journal of Geophysical Research: Space Physics*, *123*, 5452–5463. https://doi.org/10.1029/2018JA025443

Ohtani, S., Takahashi, K., & Lui, A. T. Y. (2002). Electron dynamics in the current disruption system. *Journal of Geophysical Research*, *107*(A10), 1322. https://doi.org/10.1029/2001JA009236

Ohtani, S., Takahashi, K., Zanetti, L. J., Potemra, T. A., McEntire, R. W., & Iijima, T. (1992b). Initial signatures of magnetic field and energetic particle fluxes at tail reconfiguration: Explosive growth phase. *Journal of Geophysical Research*, *97*(A12), 19324. https://doi.org/10.1029/92JA01832

Park, M. Y., Lee, D.-Y., Ohtani, S., & Kim, K. C. (2010). Statistical characteristics and significance of low-frequency instability associated with magnetic dipolarizations in the near-Earth plasma sheet. *Journal of Geophysical Research*, *115*, A11203. https://doi.org/10.1029/2010JA015566

Pu, Z. Y., Kang, K. B., Korth, A., Fu, S. Y., Zong, Q. G., Chen, Z. X., et al. (1999). Ballooning instability in the presence of a plasma flow: A synthesis of tail reconnection and current disruption models for the initiation of substorms. *Journal of Geophysical Research*, *104*(A5), 10248. https://doi.org/10.1029/1998JA900104

Pu, Z. Y., Korth, A., Chen, Z. X., Friedel, R. H. W., Zong, Q. G., Wang, X. M., et al. (1997). MHD drift ballooning instability near the inner edge of the near-Earth plasma sheet and its application to substorm onset. *Journal of Geophysical Research*, *102*(A7), 14397–14406. https://doi.org/10.1029/97JA00772

Roux, A., Perraut, S., Robert, P., Morane, A., Pedersen, A., Korth, A., et al. (1991). Plasma sheet instability related to the westward traveling surge. *Journal of Geophysical Research*, *96*(A10), 17714. https://doi.org/10.1029/91JA01106

Runov, A., Angelopoulos, V., Sitnov, M. I., Sergeev, V. A., Bonnell, J., McFadden, J. P., et al. (2009). THEMIS observations of an earthward-propagating dipolarization front. *Geophysical Research Letters*, *36*, L14106. https://doi.org/10.1029/2009GL038980

Saito, M. H., Miyashita, Y., Fujimoto, M., Shinohara, I., Saito, Y., Liou, K., & Mukai, T. (2008). Ballooning mode waves prior to substorm-associated dipolarizations: Geotail observations. *Geophysical Research Letters*, *35*, L07103. https://doi.org/10.1029/2008GL033269

Saka, O., Watanabe, O., Okada, K., & Baker, D. N. (1999). A slow mode wave as a possible source of Pi 2 and associated particle precipitation: A case study. *Annales Geophysicae*, *17*(5), 674–681. https://doi.org/10.1007/s00585-999-0674-4

Samson, J. C., MacAulay, A. K., Rankin, R., Frycz, P., & Voronkov, I. (1996). Substorm intensifications and resistive shear flow-ballooning instabilities in the near-Earth magnetotail. In *Proceedings of the third International Conference on substorms* (pp. 399–404). International conference on substorms. Noordwijk, Netherlands: European Space Agency.

Southwood, D. J., & Saunders, M. A. (1985). Curvature coupling of slow and Alfvén MHD waves in a magnetotail field configuration. *Planetary and Space Science*, *33*(1), 127–134. https://doi.org/10.1016/0032-0633(85)90149-7

Tsyganenko, N. A. (1995). Modeling the Earth's magnetospheric magnetic field confined within a realistic magnetopause. *Journal of Geophysical Research*, *100*(A4), 5599–5612. https://doi.org/10.1029/94JA03193

Turner, D. L., Claudepierre, S. G., Fennell, J. F., O'Brien, T. P., Blake, J. B., Lemon, C., et al. (2015). Energetic electron injections deep into the inner magnetosphere associated with substorm activity. *Geophysical Research Letters*, *42*, 2079–2087. https://doi.org/10.1002/2015GL063225

Voronkov, I., Rankin, R., Frycz, P., Tikhonchuk, V. T., & Samson, J. C. (1997). Coupling of shear flow and pressure gradient instabilities. *Journal of Geophysical Research*, *102*(A5), 9639–9650. https://doi.org/10.1029/97JA00386

Wang, C.-P., Xing, X., Bortnik, J., & Chu, X. (2020). Inward propagation of flow-generated Pi2 waves from the plasma sheet to the inner magnetosphere. *Journal of Geophysical Research: Space Physics*, *125*, e2019JA027581. https://doi.org/10.1029/2019JA027581

Wang, S.-Y., Kazama, Y., Jun, C.-W., Chang, T.-F., Hori, T., Miyoshi, Y., & Shinohara, I. (2018). *The LEPe instrument Level-2 3-D flux data of Exploration of energization and Radiation in Geospace (ERG) Arase satellite, Version v02_02*. ERG Science Center, Institute for Space-Earth Environmental Research, Nagoya University. https://doi.org/10.34515/DATA.ERG-04001

Xing, X., Liang, J., Spanswick, E., Lyons, L., & Angelopoulos, V. (2013). Auroral wave structures and ballooning instabilities in the plasma sheet. *Journal of Geophysical Research: Space Physics*, *118*, 6319–6326. https://doi.org/10.1002/2013JA019068

Yamamoto, M., Ozaki, M., Yamagishi, H., Taguchi, M., & Kadokura, A. (2008). Upper atmosphere physics data obtained at Syowa station in 2006. In *Japanese Antarctic Research Expedition data Reports, No. 303 (Upper atmosphere Physics)* (Vol.26, pp. 1–59). Tokyo:National Institute of Polar Research.

Yang, J., Cao, J. B., Fu, H. S., Wang, T. Y., Liu, W. L., & Yao, Z. H. (2017). Broadband high-frequency waves detected at dipolarization fronts. *Journal of Geophysical Research: Space Physics*, *122*, 4299–4307. https://doi.org/10.1002/2016JA023465

Yao, Z., Rae, I. J., Lui, A. T. Y., Murphy, K. R., Owen, C. J., Pu, Z. Y., et al. (2017). An explanation of auroral intensification during the substorm expansion phase. *Journal of Geophysical Research: Space Physics*, *122*, 8560–8576. https://doi.org/10.1002/2017JA024029

Yokota, S., Kasahara, S., Hori, T., Keika, K., Miyoshi, Y., & Shinohara, I. (2018). *The MEP-i instrument Level-2 3-D flux data of Exploration of energization and Radiation in Geospace (ERG) Arase satellite, Version v01_02*. ERG Science Center, Institute for Space-Earth Environmental Research, Nagoya University. https://doi.org/10.34515/DATA.ERG-03000

Yokota, S., Kasahara, S., Mitani, T., Asamura, K., Hirahara, M., Takashima, T., et al. (2017). Medium-energy particle experiments-ion mass analyzer (MEP-i) onboard ERG (Arase). *Earth Planets and Space*, *69*, 172. https://doi.org/10.1186/s40623-017-0754-8